

G O J A Y

Johns Hopkins

Peaking Jay AIAA Report

DBF
26

1. Executive Summary

This report outlines the design, analysis, manufacturing, and testing of the “Peaking Jay” by the Johns Hopkins team in preparation for the 2026 AIAA Design, Build, Fly (DBF) Competition. The objective is to complete three aerial missions and one ground mission, with a focus on payload capacity, banner deployment, and banner release.

The aircraft's development followed a three-phase design approach: conceptual, preliminary, and detailed. Throughout these stages, design requirements were incorporated into trade studies, and score analyses were conducted to determine the aircraft's final configuration. Emphasis was placed on the plane's weight, ease of manufacturing, and payload access to accommodate additional cargo and passengers, as specified by the mission. Balanced consideration was given to drag, lift, and stability, as the team focused on mission completion rather than speed. The trade study and score analysis led to the adoption of a 10.4 lb monoplane single-propeller tractor with a conventional empennage, taildragger landing gear, and a wing with a chord length of 10" and a span of 58", which should serve as the baseline aircraft configuration for this year's competition. A cargo bay accessed from the nose holds 8 hockey pucks in a quick-load tray in the lower half of the fuselage. The passenger compartment holds 24 ducks just above the cargo bay in grouped restraint bays. Flight electronics lie at the nose of the plane. Under the cargo bay of the fuselage lies a 2 x 10-foot banner that will be deployed and released in-flight. This year's material selection primarily uses carbon fiber sheets, balsa, plywood, and 3D-printed PLA. Manufacturing methods include laser cutting, 3D printing, and several new techniques for the team, including CNC routing, CNC hot-wire cutting, and carbon fiber wet layup. The team will test individual components, followed by ground and flight tests to validate the plane's structural integrity, control systems, and propulsion systems.

The Peaking Jay (Figure 1.1) is designed to maximize score across the three missions. For Mission 1 (M1), the team will complete 3 laps in under two minutes, with a top flight speed of 97 ft/s. In Mission 2 (M2), the team will load passengers and cargo to full capacity (4.8 lb), resulting in a takeoff weight of 15.2 lb. The aircraft will cruise at 92 ft/s, completing 7 laps in the 5-minute window, resulting in a net income of 742. For Mission 3 (M3), the aircraft will cruise at 84 ft/s carrying only the banner, completing 5 laps in the 5-minute window, resulting in an unnormalized score of 286.

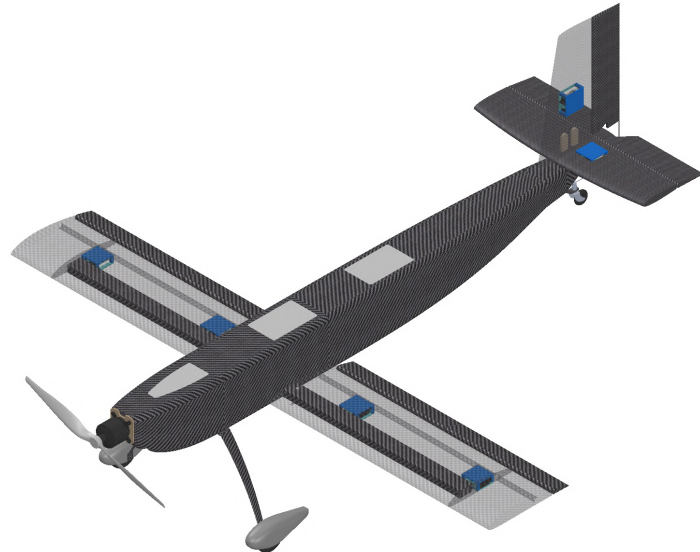


Figure 1.1: The Peaking Jay CAD render.

2. Management Summary

The student-led Johns Hopkins University Design, Build Fly (DBF) team comprises 15 undergraduates, 11 of whom are underclassmen. The team is supported by a faculty advisor, two industry advisors, and three graduate advisors, all of whom participate in key design reviews. Financially, the team is supported by grants from the Johns Hopkins University Department of Mechanical Engineering and sponsorships from private companies.

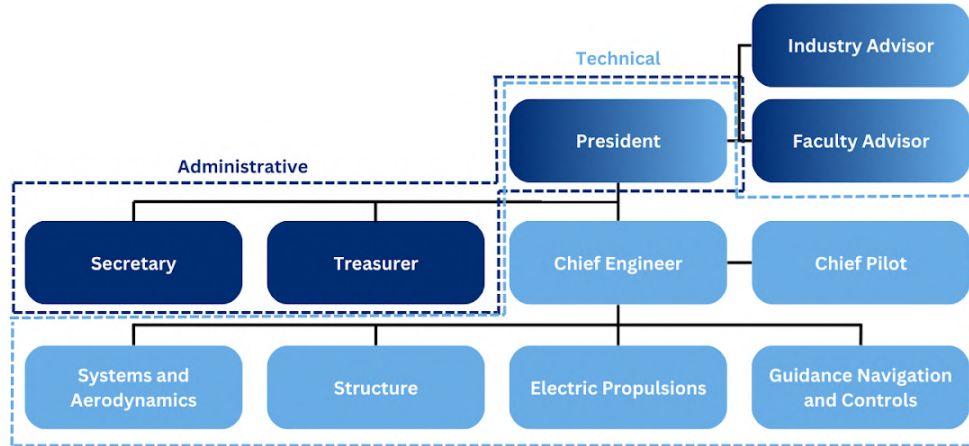


Figure 2.1: Management hierarchy.

2.1 Team Organization

The JHU DBF team consists of 15 undergraduate members organized into advisory, administrative, and technical branches. The team is supported by a Faculty and an Industry Advisor who provide strategic guidance, technical mentorship, and oversight throughout the design, manufacturing, and testing phases.

The administrative branch is led by the President and supported by the Secretary and Treasurer. This group manages organizational planning, financial oversight, documentation, and external coordination. The President ensures alignment between project milestones, competition requirements, and advisory direction while maintaining overall team operations.

The technical branch is led by the Chief Engineer, who serves as the primary technical authority for the aircraft. The Chief Engineer directs all aspects of design, integration, and validation and directly manages the four technical subteams: Systems and Aerodynamics, which conducts aircraft sizing and performance analysis; Structures, which oversees structural design and load validation; Electric Propulsions, which manages propulsion system integration and power configuration; and Guidance, Navigation, and Controls (GNC), which supports flight control implementation and stability development.

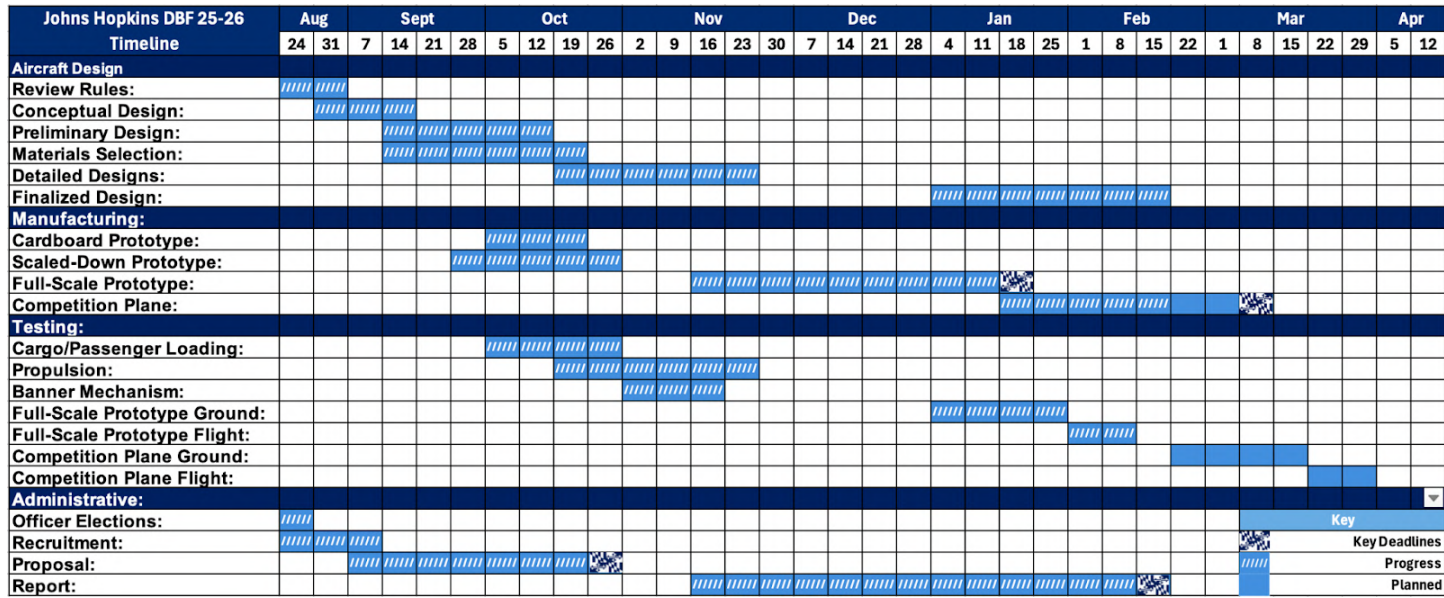
The Chief Pilot works closely with the Chief Engineer to support flight readiness and competition operations. Significant cross-subsystem design decisions are discussed in full-team integration meetings, with final authority retained by the Chief Engineer to maintain schedule and configuration control.

When technical conflicts arise, an internal group discussion will proceed in which participants are open to sharing ideas, and a general consensus will be reached through a simple vote. This process is for cross-subteam conflicts; these conflicts are brought to the Chief Engineer and discussed during a full team meeting, where, if no consensus is reached, the Chief Engineer has the authority to make a final decision. Leadership-level disputes are resolved through similar conversations with faculty and industry advisors whenever necessary.

2.2 Design Schedule

The Gantt chart in Table 2.1 was created at the start of the semester and guides the Chief Engineer and the Secretary in preparing for the competition. The Chief Engineer oversees the subteam leads to meet the developmental deadlines for design, manufacturing, and testing. The Secretary works with the team, overseeing administrative and procedural deadlines, primarily on the proposal and report. The whole team refers to the Gantt Chart during weekly General Body meetings to address potential roadblocks that could delay critical deadlines. The key deadlines encompass both developmental and administrative deadlines: a complete full-scale prototype, the competition aircraft, the proposal, and the report. Progress so far has been on schedule, without any week-long delays to the project.

Table 2.1: Team Gantt chart.



3. Conceptual Design

3.1 Problem Statement

The aircraft's purpose is a banner-towing bush plane. For this, the plane must be capable of carrying both passengers and cargo, as well as a banner that can be remotely deployed and released. The flight missions simulate these conditions by requiring proof of flight capabilities (M1), conducting a charter flight (M2) using rubber ducks as passengers and hockey pucks as cargo, and conducting a banner flight (M3) to deploy

and release a banner mid-flight. Additionally, loading and unloading the payload must be quick (GM). Overall success depends on optimizing the aircraft for the key characteristics outlined in the following sections.

3.1.1 Mission Scoring

As outlined in the competition rules [1], the total score (Competition Score) is based on the Proposal Score, Design Report Score, Total Mission Score, and the Participation Score. The participation score is 1 for attending the flyoff, 2 for completing the tech inspection, and 3 for attempting a flight mission.

$$(3.1) \quad \text{Competition Score} = \text{Total Report Score} \times \text{Total Mission Score} + \text{Participation Score}$$

$$(3.2) \quad \text{Total Report Score} = 0.15 \times \text{Proposal Score} + 0.85 \times \text{Design Report Score}$$

$$(3.3) \quad \text{Total Mission Score} = M1 + M2 + M3 + GM$$

All flight missions fly around the same course, as depicted in Figure 3.1. Details on mission requirements and awarded points are outlined in the following sections.

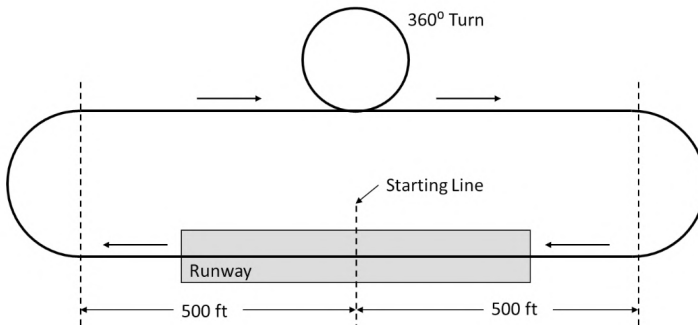


Figure 3.1: Flight course.

3.1.2 Ground Mission

GM involves loading and unloading all of the payload used across missions 2 and 3. Points are awarded based on the time it takes to complete the ground mission, normalized to the fastest team.

$$(3.4) \quad GM = \frac{\text{MissionTime}_{Min}}{\text{MissionTime}_{JHU}}$$

3.1.3 Mission 1 - Test Flight

M1 involves completing 3 laps of the flight course in a 5-minute window. Upon completion, 1 point is granted.

$$(3.5) \quad M1 = 1$$

3.1.4 Mission 2 - Charter Flight

M2 involves carrying passengers and cargo and completing as many laps as possible. Points are awarded based on Net Income, determined by the following equations.

$$(3.6) \quad NetIncome = Income - Cost$$

$$(3.7) \quad Income = [\#Passengers \times (6 + (2 \times \#Laps))] + [\#Cargo \times (10 + (8 \times \#Laps))]$$

$$(3.8) \quad Cost = \#Laps \times (10 + (\#Passengers \times 0.5) + (\#Cargo \times 2) \times EF)$$

$$(3.9) \quad EF = Efficiency Factor = Total Propulsion Battery Capacity (W-hrs) / 100$$

Points earned for M2 are the net income normalized to the most profitable team, plus one point for successfully completing the mission.

$$(3.10) \quad M2 = 1 + \frac{NetIncome_{JHU}}{NetIncome_{Max}}$$

3.1.5 Mission 3 - Banner Flight

M3 involves taking off with a banner attached to the aircraft. The banner is deployed remotely mid-flight and towed by the plane. Once five minutes have elapsed, the banner is released from the plane, which then drops to the ground, and the plane must successfully land. Scoring is based on the number of laps completed, the banner length, and the RAC, defined below. Again, this value is normalized to the team with the highest score. An additional 2 points are awarded for successfully completing the mission.

$$(3.11) \quad RAC = 0.05 \times \frac{Wingspan \text{ (in)}}{12} + 0.75$$

$$(3.12) \quad M3 = 2 + \frac{[\#Laps \times BannerLength / RAC]_{JHU}}{[\#Laps \times BannerLength / RAC]_{Max}}$$

3.2 Subsystem Design Requirements

Sub-systems are split into fuselage, wing & empennage, payload, and propulsion. This subsystem model ensures modularity in the design of the plane for isolating tasks while maintaining ease of integrating systems. The relevant mission objectives and requirements are distributed to each subsystem.

Table 3.1: Subsystem Requirements.

| Subsystem | Requirement |
|------------------|------------------------------------------------------------------------------------------|
| Fuselage | Structures must be strong enough to handle heavy payload and maximum G's. |
| | The fuselage must be large enough to fit the payload and propulsion systems. |
| | Weight must be minimized to increase payload capacity. |
| Wing & Empennage | C_L must be large to accommodate a heavy payload. |
| | C_d must be low to allow for fast lap times. |
| | Wingspan must be optimized to minimize RAC, while staying within the 3'-5' wingspan. |
| Payload | Payload loading must be made quick and easy. But passengers must be loaded individually. |
| | Payload system must be optimized to fit passengers and cargo in a small space. |

| | |
|------------|-----------------------------------------------------------------------------------------------------------------------------------------------------------------------------------------------------------------------------------------------------------------------------------------------------------------------|
| | Passenger area must be isolated from cargo, wiring, etc., accessible only by a door or hatch. Passengers and cargo must be restrained during flight to prevent movement. Passenger and cargo quantities must be optimized. Banner mechanism must secure the banner in place to prevent premature deployment. |
| Propulsion | Flight must be sustained for the full 5-minute mission duration. |
| | Motor must be strong enough to pull the desired payload and gain speed to generate lift. |
| | Total battery capacity must be minimized to reduce the Efficiency Factor. |

3.3 Scoring Sensitivity Analysis

To guide aircraft requirements prioritization, a scoring sensitivity analysis was conducted. This highlighted key factors that have a greater impact on the final scoring that we could focus our efforts on, while setting aside less important factors. Utilizing Python [2], we graphed how percent changes in each individual variable in the relevant scoring equation change the overall score for that mission.

GM and M1 are uninteresting as GM is only based on the time to complete the mission, so it was trivially decided that the ability to quickly load/unload payload is prioritized. M1 is a flat score for completing the mission, requiring no specialized optimizations.

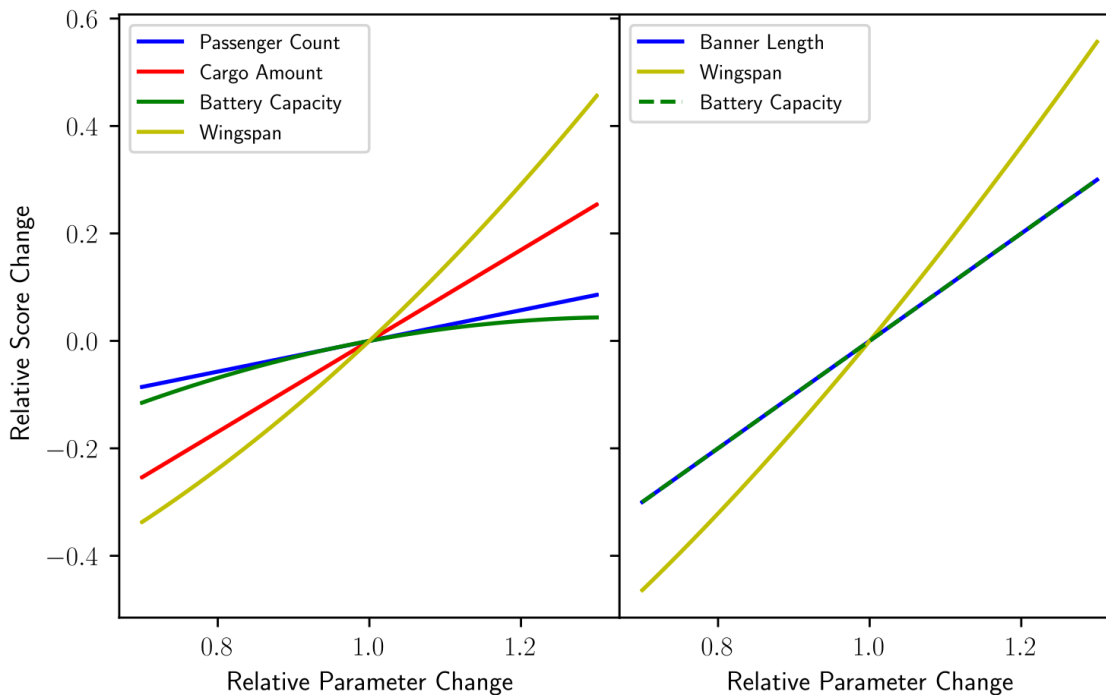


Figure 3.2: Mission 2 Sensitivity.

Figure 3.3: Mission 3 Sensitivity.

M2 is based on a variety of factors, as outlined in section 3.1.4. Figure 3.2 shows how changing key variables by up to $\pm 30\%$ affects the score. Wingspan and battery capacity affect mission performance

indirectly, so relevant variables such as thrust, C_L , and C_d were calculated to estimate #Laps (see Eqs. 3.7 and 3.8) and to measure their impact on the final score. The primary factor in scoring was wingspan. Although increased drag penalizes larger wingspans, the additional endurance to complete more laps outweighs the downsides. The second most important factor for scoring is cargo capacity. Though it substantially increases total weight and thus decreases endurance, increased cargo capacity drastically increases net income.

M3 was similarly analyzed (Figure 3.3), with banner length, wingspan, and battery capacity compared. Wingspan was found to be the largest factor because of its inclusion in the RAC score; however, this directly conflicts with M2's objectives. As a result, we elected to forego minimizing the M3 score in favor of achieving a higher M2 score. Though optimization in both missions nets the same potential points, M2 is more likely to be flown at all because it is flown first. The next most important factor was maximizing the banner length. This became the primary focus for maximizing M3's score. Figure 3.4 shows the breakdown of drag and thrust provided by the propeller, with the red point indicating the maximum cruise speed with the banner, and the blue point indicating it without the banner.

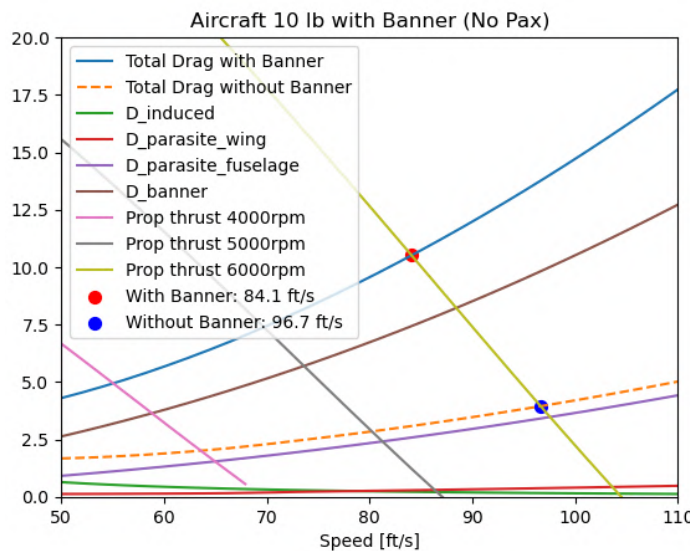


Figure 3.4: Aircraft flight speed parameters analysis.

3.4 Configuration Selection

3.4.1 Wing Type

Biplane, flying-wing, and monoplane configurations were considered for the aircraft's wing type. The appropriate figures of merit for the decision were stability, drag reduction, lift, manufacturability, and weight. Stability and weight were identified as the most critical factors influencing overall aircraft flight, especially with the added weight of payload. Given this, a monoplane was deemed to be the best decision for this year's aircraft because it performs highly in all categories considered.

Table 3.2: Wing type decision matrix.

| Figure of Merit | Factor | Biplane | Flying Wing | Monoplane |
|--------------------------|--------------|------------|-------------|-------------|
| Stability | 0.60 | 7 | 3 | 7 |
| Drag Reduction | 0.30 | 4 | 8 | 6 |
| Lift | 0.30 | 8 | 4 | 7 |
| Manufacturability | 0.20 | 3 | 7 | 8 |
| Weight | 0.50 | 3 | 8 | 7 |
| | TOTAL | 9.9 | 10.8 | 13.2 |

3.4.2 Wing Position

There were four considerations regarding the wing's position on the aircraft: a low-wing, mid-wing, high-wing, or parasol wing. With these considerations in mind, the relevant figures of merit are stability, manufacturability, and payload access. Our primary concern was payload access, given the GM score, and then stability to accommodate the added payload weight. We ultimately decided on a low-wing as the best design choice given its payload access score. The manufacturability proved simpler than other options, and it provides adequate stability for the payload weight.

Table 3.3: Wing position decision matrix.

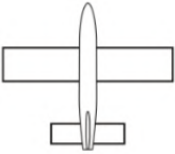
| | |  |  |  |  |
|--------------------------|--------------|-------------------------------------------------------------------------------------|--------------------------------------------------------------------------------------|---------------------------------------------------------------------------------------|---------------------------------------------------------------------------------------|
| Figure of Merit | Factor | Low Wing | Mid Wing | High Wing | Parasol Wing |
| Stability | 0.30 | 4 | 6 | 8 | 7 |
| Manufacturability | 0.25 | 9 | 7 | 8 | 3 |
| Payload Access | 0.45 | 8 | 3 | 5 | 6 |
| | TOTAL | 7.05 | 4.90 | 6.65 | 5.55 |

3.4.3 Wing Shape

When choosing the shape of the wing, there were four that were in consideration: constant chord, tapered, reverse tapered, and compound tapered. The appropriate figures of merit considered were manufacturability, lift, stability, and the drag reduction of these wing shapes. The most important factors were lift and stability. Similar to the reasoning for the wing position, we wanted to maximize the plane's lift and stability, given the added weight of passengers, cargo, and banner mechanisms. The finalized shape was the

constant chord because, while not the leading choice for drag reduction, it is good for both lift and stability and is highly manufacturable.

Table 3.4: Wing shape decision matrix.

| | |  |  |  |  |
|-------------------|--------------|-----------------------------------------------------------------------------------|------------------------------------------------------------------------------------|-------------------------------------------------------------------------------------|-------------------------------------------------------------------------------------|
| Figure of Merit | Factor | Constant Chord | Tapered | Reverse Tapered | Compound Tapered |
| Manufacturability | 0.75 | 10 | 8 | 6 | 7 |
| Lift | 0.5 | 8 | 9 | 9 | 9 |
| Stability | 0.4 | 8 | 4 | 8 | 4 |
| Drag | 0.25 | 2 | 8 | 5 | 9 |
| | TOTAL | 15.2 | 14.1 | 13.45 | 13.6 |

3.4.4 Wing Sweep

When choosing the wing sweep, we considered four possible sweep types: straight, swept, forward-swept, and variable-swept. For this, the critical figures of merit were manufacturability, lift, stability, and drag reduction. The straight sweep was chosen for its ease of manufacturing, despite performing slightly worse than the swept wing in terms of stability and drag reduction.

Table 3.5: Wing sweep decision matrix.

| | |  |  |  |  |
|-------------------|--------------|-------------------------------------------------------------------------------------|-------------------------------------------------------------------------------------|---------------------------------------------------------------------------------------|---------------------------------------------------------------------------------------|
| Figure of Merit | Factor | Straight | Swept | Forward Swept | Variable |
| Manufacturability | 0.75 | 10 | 8 | 6 | 2 |
| Lift | 0.5 | 8 | 6 | 6 | 9 |
| Stability | 0.4 | 6 | 7 | 7 | 4 |
| Drag | 0.5 | 5 | 7 | 6 | 8 |
| | TOTAL | 16.4 | 15.3 | 13.3 | 11.6 |

3.4.5 Propulsion Configuration

The configurations considered for propulsion were single-tractor, single-pusher, twin-tractor, and twin-pusher. These configurations were assessed on their maximum thrust, efficiency, design complexity, flight characteristics, and thrust-to-weight ratio. While maximum thrust and thrust-to-weight were considered factors in selecting the configuration, they were found to be less important than the configuration's efficiency. The main reason for this decision was that maximum thrust and thrust-to-weight are most important during the takeoff phase of flight, while efficiency determines the aircraft's endurance. With a higher efficiency, higher thrust settings can be used for cruise flight, negating any power advantage that a high maximum thrust configuration would bring. Efficiency was determined by factors such as design weight and powertrain weight, which in turn influenced power consumption during flight. Flight characteristics are determined by the pitching moment caused by different thrust settings, with a higher score representing a higher center of thrust being closer to the center of mass. With these considerations, a single-tractor propulsion configuration was chosen, as it performs best in terms of efficiency, design complexity, and flight characteristics.

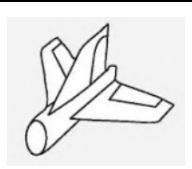
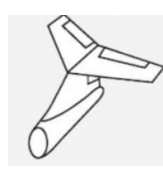
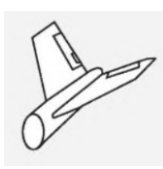
Table 3.6: Propulsion configuration decision matrix.

| Parameter | Factor | Single-Tractor | Single-Pusher | Twin-Tractor | Twin-Pusher |
|------------------------|--------------|----------------|---------------|--------------|-------------|
| Maximum Thrust | 0.15 | 7 | 6 | 10 | 9 |
| Efficiency | 0.25 | 10 | 9 | 7 | 6 |
| Design Complexity | 0.25 | 10 | 8 | 1 | 1 |
| Flight Characteristics | 0.25 | 9 | 5 | 7 | 7 |
| Thrust-to-weight | 0.1 | 10 | 10 | 6 | 6 |
| | TOTAL | 9.3 | 8.15 | 6.35 | 5.45 |

3.4.6 Tail Configuration

The conceptual design of the tail saw a potential of six designs: conventional tail, cruciform, T-tail, V-tail, and twin tail. The figures of merit were manufacturability, drag reduction, weight reduction, and stability. Our factors were mostly even for our tail shape, as we wanted it to be well-rounded overall, with a slight focus on ease of manufacturing. These considerations led to the decision to use conventional tail.

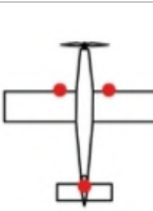
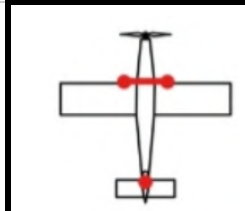
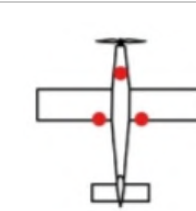
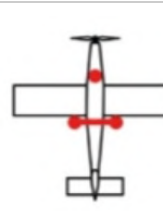
Table 3.7 Tail configuration decision matrix.

| | |  |  |  |  |  |
|------------------------------|--------------|-----------------------------------------------------------------------------------|-----------------------------------------------------------------------------------|------------------------------------------------------------------------------------|-------------------------------------------------------------------------------------|-------------------------------------------------------------------------------------|
| Figure of Merit | Factor | Conventional | Cruciform | T-Tail | V-Tail | Twin Tail |
| Ease of Manufacturing | 0.75 | 10 | 7 | 7 | 6 | 5 |
| Drag Reduction | 0.5 | 8 | 7 | 8 | 9 | 7 |
| Weight Reduction | 0.5 | 10 | 10 | 10 | 10 | 6 |
| Stability | 0.5 | 8 | 6 | 5 | 6 | 8 |
| | TOTAL | 20.5 | 16.75 | 16.75 | 17 | 14.25 |

3.4.7 Gear Configuration

For gear placement, we considered four main designs: the wing taildragger, the bow taildragger, the strut tricycle, and the bow tricycle. For this, the appropriate figures of merit were manufacturability, strength, weight, and stability. Despite a slight focus on the strength and stability, the factors are evenly distributed across these considerations. With this scale, we decided to use a bow taildragger because it was strong enough to support the passengers' and cargo's weight, while also being relatively easy to manufacture.

Table 3.8 Gear configuration decision matrix.

| | |  |  |  |  |
|------------------------------|--------------|-------------------------------------------------------------------------------------|-------------------------------------------------------------------------------------|---------------------------------------------------------------------------------------|---------------------------------------------------------------------------------------|
| Figure of Merit | Factor | Wing Taildragger | Bow Taildragger | Strut Tricycle | Bow Tricycle |
| Ease of Manufacturing | 0.75 | 6 | 8 | 6 | 6 |
| Strength | 0.5 | 7 | 7 | 5 | 8 |
| Weight | 0.4 | 8 | 8 | 7 | 7 |
| Stability | 0.5 | 7 | 6 | 8 | 6 |
| | TOTAL | 14.7 | 15.7 | 13.8 | 14.3 |

3.4.8 Banner Position

The banner positions considered were below the fuselage (longitudinal), above the fuselage (longitudinal), under the wing (lateral), or under the tail. The appropriate figures of merit for this were the ease of assembly, reliability, and drag reduction. We determined that reliability was highest for M3 scoring, followed by ease of assembly for GM scoring. Ultimately, the banner is stowed longitudinally beneath the fuselage due to its high scores for ease of assembly and reliability.

Table 3.9: Banner position decision matrix.

| Figure of Merit | Factor | Below Fuselage (Longitudinal) | Above Fuselage (Longitudinal) | Under Wing (Lateral) | Under Tail |
|------------------|--------------|----------------------------------|----------------------------------|-------------------------|------------|
| Ease of Assembly | 0.4 | 8 | 4 | 7 | 5 |
| Reliability | 0.6 | 7 | 3 | 5 | 6 |
| Drag Reduction | 0.2 | 6 | 6 | 3 | 8 |
| | TOTAL | 8.6 | 4.6 | 6.4 | 7.2 |

3.4.9 Banner Material

The team has reviewed previous DBF reports from past competitions to determine the optimal material for the banner. The materials considered for the banner were Icarex polyester, Kevlar, low-density polyethylene (LDPE), peel ply, and ripstop nylon. To make an appropriate selection, the mission-critical characteristics were drag reduction, density, and stiffness. Emphasis was placed on density to reduce the aircraft's overall weight, and stiffness was deemed important to allow the banner to fly longitudinally and keep the logo visible, as per mission requirements. Therefore, our final decision was ripstop nylon due to its performance in weight reduction, increased stiffness, and reduced drag.

Table 3.10: Banner material decision matrix.

| Figure of Merit | Factor | Icarex Polyester | Kevlar | Low-Density Polyethylene (LDPE) | Peel Ply | Ripstop Nylon |
|-----------------|--------------|------------------|------------|------------------------------------|------------|---------------|
| Drag Reduction | 0.4 | 7 | 3 | 6 | 4 | 8 |
| Density | 0.7 | 6 | 4 | 8 | 6 | 7 |
| Stiffness | 0.5 | 7 | 7 | 3 | 4 | 8 |
| | TOTAL | 10.5 | 7.5 | 9.5 | 7.8 | 12.1 |

3.5 Final Configuration

The final aircraft is a low-wing monoplane with a single-propeller tractor, a conventional tail, and a taildragger that stows a banner below the fuselage. The conceptual drawing with all chosen parts together is displayed in Figure 3.5.



Figure 3.5: Final aircraft configuration.

4. Preliminary Design

The preliminary design is the culmination of iterative ideas that converge on an optimal solution for carrying passengers, cargo, and the banner. Trade studies, sensitivity analyses, and simulations were used in conjunction to inform the decision-making process. Details of these processes are outlined in this section.

4.1 Design Methodology

The design methodology is shown in Figure 4.1. Based on mission requirements and design constraints, an initial aircraft configuration was selected through trade studies. Sensitivity analysis was conducted in Jupyter notebooks with Python as the kernel. AirfoilDatabase enabled us to calculate wing performance, while overall aircraft performance was determined through hand calculations and Python numerical methods. The phase following conceptual design is preliminary design, during which the weights and locations of critical flight components are established to maintain a constant CG location. Configurations were sketched during team meetings, and then designs were drafted in SolidWorks. Theoretical performance data is collected through previous testing and calculus. Once a viable design had been developed, a prototype aircraft was built to verify the predicted performance. Actual performance data was then used to iterate on future revisions of the aircraft, allowing for higher performance and improved serviceability.

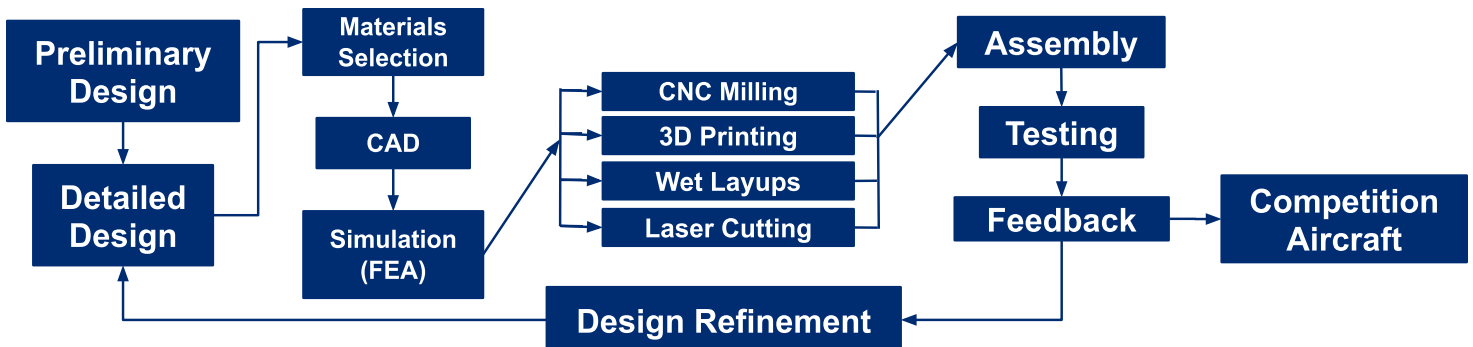


Figure 4.1: Design methodology.

4.2 Trade Studies

4.2.1 Airfoil Selection

The two scenarios that received special consideration in the airfoil selection were cruising with a heavy payload (M2) and high-drag cruising (M3). For heavy cruising, the main characteristics for airfoil selection were C_L near critical angle of attack, representing lifting capacity, C_L/C_d near critical angle of attack, representing airfoil efficiency, and the range of which C_L stayed high near critical angle of attack, representing airfoil stall characteristics. For high drag cruising, C_L/C_d near an angle of attack of 0° was considered. Aerodynamic characteristics were simulated with a Reynolds number of 150,000 for all missions.

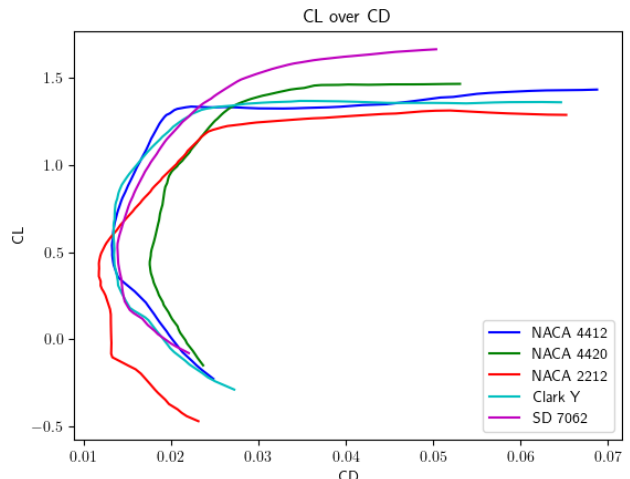
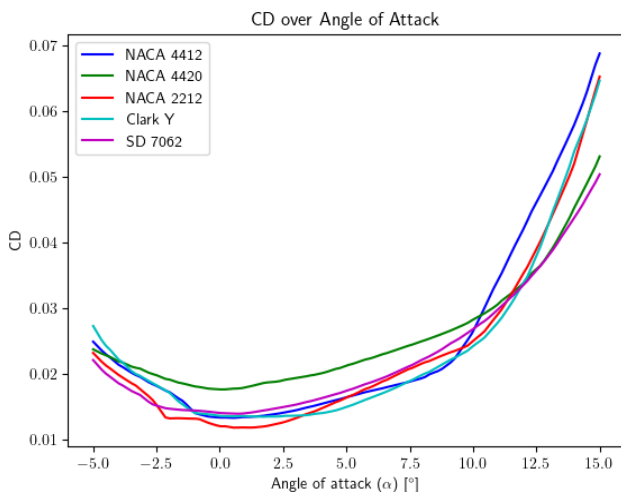
Figure 4.2: C_L/C_d of Airfoil.

Figure 4.3: Airfoil drag across angle of attack.

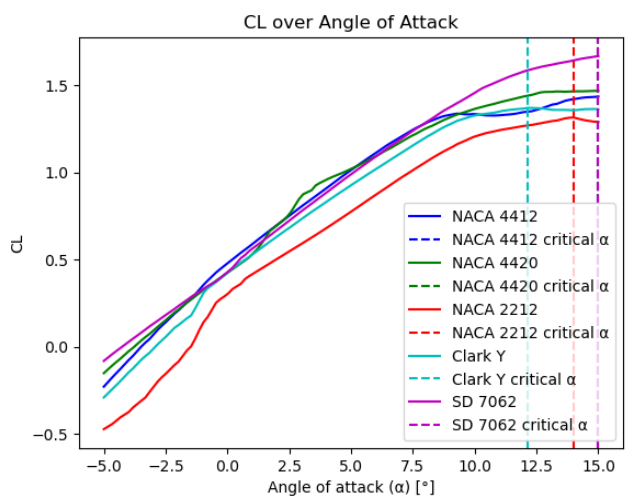


Figure 4.4: Airfoil lift across angle of attack.

Based on these considerations, we have selected five candidate airfoils: NACA 4412, NACA 4420, NACA 2212, Clark Y, and SD 7062. We have found no significant deviations in manufacturing cost and complexity between the airfoils. We have found that NACA 4412 exhibits superior aerodynamic performance, including airfoil efficiency and lifting capacity, across a wide range of flight conditions.

Table 4.1: Airfoil decision matrix.

| Parameter | Factor | NACA 4412 | NACA 4420 | NACA 2212 | Clark Y | SD 7062 |
|------------------------------------|--------------|-----------|-------------|-------------|------------|-------------|
| $C_L @ \alpha \rightarrow 0^\circ$ | 0.1 | 5 | 3 | 1 | 3 | 4 |
| C_L vs α | 0.3 | 3 | 4 | 1 | 2 | 5 |
| C_D vs α | 0.15 | 3 | 2 | 4 | 3 | 3 |
| C_L/C_D vs α | 0.4 | 5 | 1 | 1 | 4 | 3 |
| Stall Stability | 0.05 | 3 | 5 | 1 | 5 | 4 |
| | TOTAL | 4 | 2.45 | 1.45 | 3.2 | 3.75 |

4.2.2 Empennage Sizing

An aircraft with high payload capacity and stability was desired. Because the aircraft is a low-wing taildragger, it is more sensitive to CG variation and pitch behavior. The equations for horizontal (V_h) and vertical tail volume coefficients (V_v) are given in Equations 4.1 and 4.2, where L_h is the horizontal tail moment arm, L_v is the vertical tail moment arm, S_w is the wing area, b is the wing span, and c is the chord length. The team has chosen to proceed with a high V_h to provide sufficient pitch authority. A relatively high horizontal tail area (S_h) was selected to provide sufficient static margin given the increased wing loading in M2 and the CG shifts in different mission configurations. The larger horizontal stabilizer improves trim flexibility and reduces sensitivity to aft-CG conditions, at the expense of an acceptable drag penalty.

Similarly, a relatively large V_v with a large vertical tail area (S_v) was chosen to ensure sufficient directional stability during banner towing operations. The banner introduces significant drag and yaw disturbances, which would be amplified in windy conditions. Therefore, high rudder authority is desired. Additionally, taildraggers are inherently more prone to directional instability during takeoff roll, making a high V_v desired.

$$(4.1) \quad V_h = \frac{S_h L_h}{S_w c}$$

$$(4.2) \quad V_v = \frac{S_v L_v}{S_w b}$$

4.2.3 Landing Gear Sizing

In sizing the landing gear for the taildragger configuration, the team followed Raymer's [3] guidance, which recommends a ground angle typically in the 10–15° range to balance propeller clearance, rotation capability, and longitudinal stability during takeoff. The ground angle is defined as the angle between the fuselage reference line and the runway when the aircraft is resting on its main and tail wheels. While this range is generally considered optimal for tailwheel aircraft, our team selected a slightly lower ground angle to create additional vertical clearance for the banner stowed beneath the fuselage. This would also provide more space for crew members to install non-permanent features to assist with banner deployment and release to the aircraft in GM and M3.

4.2.4 Passenger & Cargo Sizing

The passenger restraint system was sized based on the number of passengers and the average passenger dimensions. Based on preliminary sizing, the team has chosen to design for the maximum passenger and cargo capacity. Additionally, to maintain the 1:3 ratio of cargo to passengers and to ensure compatibility with the fuselage cross-section in all sections, the team has decided to partition the fuselage into a top and bottom deck, with the top deck housing passengers and the bottom deck housing cargo. This decision was also influenced by the cargo's weight, as placing the heavier cargo lower and closer to the CG would reduce the unstable moment induced during roll operations. Additionally, the taper at the rear of the fuselage reduced the available space for additional passengers. To select the optimal restraint systems for both the passengers and the cargo, a trade study has been conducted and presented in Table 4.2:

Table 4.2: Passenger and cargo restraint selection process.

| | Restraint Mechanism | |
|--------------|------------------------------------------------------------------------------------------------------------------------------------------------------------------|------------------------------------------------------------------------------------------------------------------------------------------------|
| | Elastic fixture | Rigid Fixture |
| Payload Type | Flexible holder that adapts its grip using material elasticity | Fixed-geometry holder that does not deform, precisely sized for the part |
| Passengers | Pros: Adapts to passengers of different sizes, better grip on soft surfaces Cons: Low positional precision, high design complexity, material prone to failure | Pros: Durable, easier design process Cons: May damage passengers, risk of slipping if geometry mismatch, requires fixtures of various sizes |
| Cargo | Pros: Provides shock absorption, higher tolerance to minor dimensional variation Cons: Overdesign for uniform objects | Pros: Repeatability and alignment, simple and low-cost design Cons: Less flexibility if puck dimensions vary |

Although it required greater design effort, an elastic fixture that better adapts to variations in passenger geometry and dimensions was deemed optimal for the passenger restraint mechanism. On the other hand, a rigid fixture was deemed optimal for the cargo restraint mechanism.

In summary, the passenger compartment measured 35.05" long, 4.125" wide, and 3.06" tall. The cargo compartment measured 26" long, 3.5" wide, and 1.16" tall.

4.2.5 Fuselage Sizing

The fuselage sizing process was driven by the payload volume, payload weight distribution, and structural requirements. The decision to position passengers on the top deck resulted in a smooth, straight surface to accommodate the large number of passengers, extending beyond the avionics bay to the empennage section. The heavier cargo was positioned near the CG, and due to its lower volume, a taper to the bottom fuselage surface was designed to reduce weight and ensure efficient usage of internal space. Bulkheads were placed along the fuselage length to resist buckling, while multiple openings on the fuselage surface were designed for maintenance and access. These bulkheads would also guide the loading of cargo and passengers.

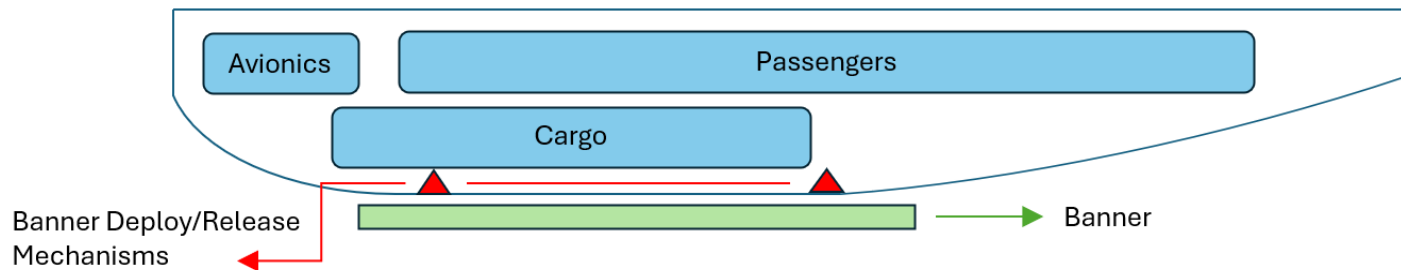


Figure 4.5: Fuselage layout with payload and avionics.

4.2.6 Banner Sizing

Research done by Rubin D. and Morr (1978) examines the relationship between banner aspect ratio and drag [4]. It was found that a long and narrow banner with a high aspect ratio results in lower drag. Due to the maximum aspect ratio of 5:1, the team has chosen the highest permitted value. The width was set to 2 ft, approximately half the fuselage length. A greater width requires more ground clearance, leading to a suboptimal ground angle for the taildragger and difficulties mounting deploy-and-release mechanisms for the banner. This led us to converge on a banner width of 2 ft and a length of 10 ft.

4.3 Aircraft Performance

4.3.1 Lift and Drag Analysis

The aircraft's aerodynamic characteristics were modeled to ensure that mission requirements for speed and payload capacity were met while maintaining structural integrity. By utilizing fully composite construction, the airframe benefits from reduced skin friction and an improved surface finish, which directly influence the parasitic drag profile. The total drag coefficient C_d was modeled using a standard drag polar approach, accounting for both zero-lift drag and lift-induced drag. Based on the composite manufacturing process, the parasitic drag coefficient $C_{d,0}$ was estimated at 0.035. The induced drag was calculated using the Oswald efficiency factor ($e = 0.80$) and the aircraft's aspect ratio ($AR = 5.9$). The resulting drag polar equation used for mission planning is:

$$(4.3) \quad C_d = 0.032 + 0.0647C_l^2$$

Lift and drag requirements were evaluated at the target cruise speeds for each mission. As shown in Table 4.3, M2 represents the most critical aerodynamic state due to the increased wing loading.

Table 4.3: Cruise speed, lift, and drag across missions

| Mission | Cruise Speed (ft/s) | C_L | C_d |
|---------|---------------------|-------|-------|
| M1 | 80 | 0.345 | 0.04 |
| M2 | 92 | 0.377 | 0.042 |
| M3 | 84 | 0.33 | 0.039 |

The relationship between velocity and aerodynamic forces is presented in the force buildup plots (Figure 4.6 & Figure 4.7). In the M2 configuration, the point at which parasitic and induced drag are equal occurs at approximately 94 ft/s. This confirms that the selected mission cruise speed of 92 ft/s is well-aligned.

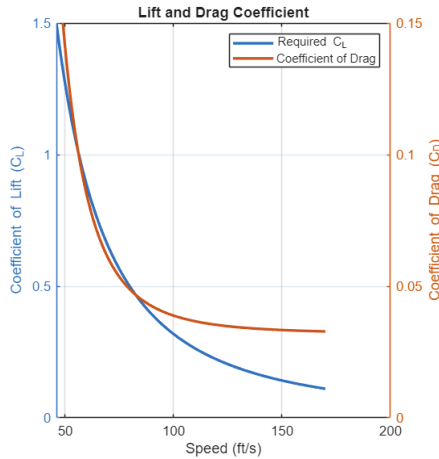


Figure 4.6: Lift and drag coefficient vs. speeds.

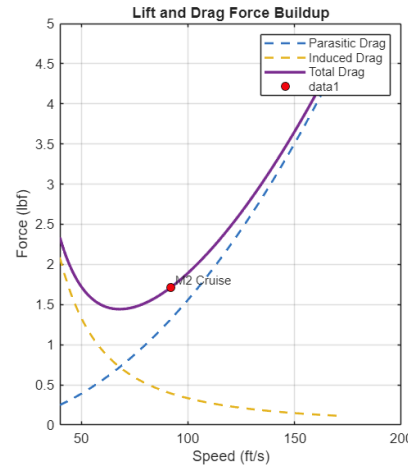


Figure 4.7: Lift and drag force buildup across speeds.

4.4 Aircraft Stability

The aircraft's stability derivatives were calculated in AVL [5]. The geometry of the wing and tail was modeled and used as the input. The figure on the right verifies that the correct geometry was used as an input. The left graph shows that all loci are on the left side of the y-axis, showing the aircraft is stable in all modes.

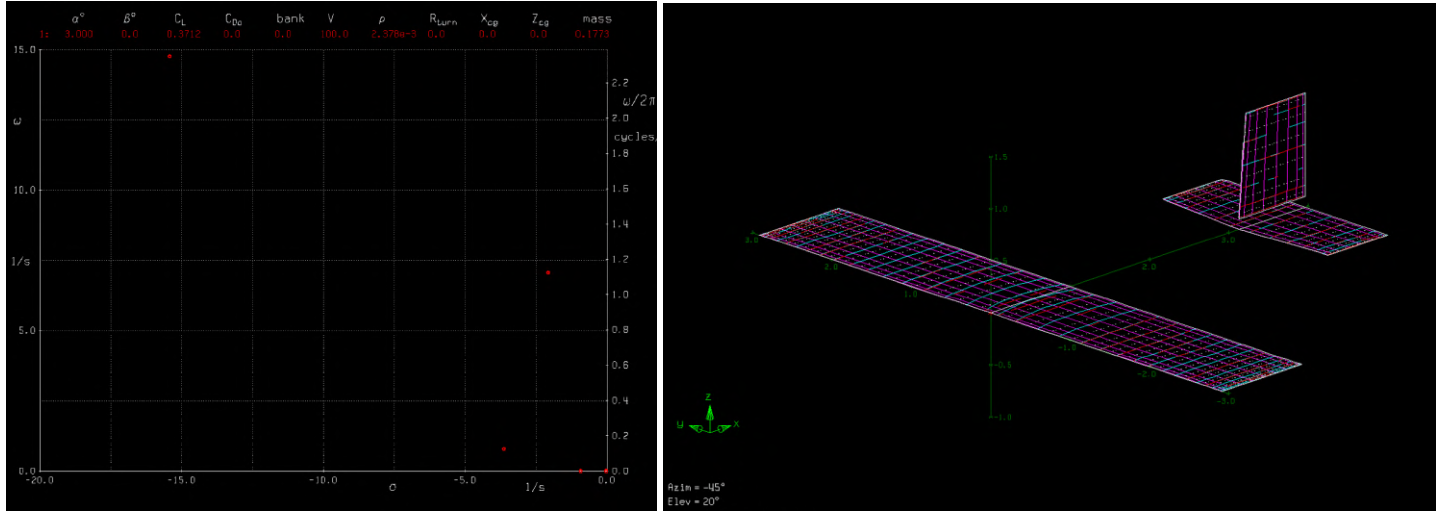


Figure 4.8: Aircraft stability analyses in AVL.

5. Detail Design

5.1 Dimensional Aircraft Parameters

An overview of the final dimensions of the aircraft is shown in Table 5.1.

Table 5.1: Aircraft sizing parameters.

| Fuselage | | Control Surfaces | | | | |
|-----------------------|----------------------|------------------|------------|-----------|--------------|----------|
| Total Length | 57.13 in | | Ailerons | Flaps | Elevator | Rudder |
| Max Width | 5.00 in | Span | 13.33 in | 13.33 in | 20.94 in | 12.6 in |
| Max Height | 6.00 in | Mean Chord | 2.11 in | 2.11 in | 3.35 in | 3.35 in |
| Frontal Area | 7.37 in ² | Max Deflection | 45 deg | 30 deg | 30 deg | 30 deg |
| | Airfoil | Span | Root Chord | Tip Chord | Aspect ratio | Tail Arm |
| Vertical Stabilizer | NACA 0012 | 12.6 in | 10.00 in | 7.49 in | 2.44 | 37.20 in |
| Horizontal Stabilizer | NACA 0012 | 20.94 in | 8.33 in | 7.49 in | 3.78 | 37.42 in |
| Wing | NACA 4412 | 59.00 in | 10.00 in | 10.00 in | 5.9 | N/A |

5.2 Structural Characteristics

5.2.1 Fuselage

The CAD model of the fuselage is shown in Figure 5.1. It is fully constructed from carbon fiber, with three plies oriented at $0/90^\circ$, $\pm 45^\circ$, and $0/90^\circ$ to maximize bending and torsional stiffness. The decision to use a 3-ply configuration was based on ANSYS ACP [6] finite element analysis (FEA) results. A 6g load with a safety factor of 1.5, equivalent to 140 lbf load applied to the wing mount area, induced a maximum stress of around 73,090 psi, which is below carbon fiber's ultimate strength of 300,000 psi (Figure 5.2). Various hatches were made in the fuselage skin, including one on the top of the fuselage for access to avionics components, two for access to the passenger compartment, one for access to the cargo compartment, and one for inserting the empennage assembly. Additional FEA simulations were conducted to assess structural integrity, including a torsion test in which a moment of 150 lbf was applied. Using the maximum stress, maximum strain, and Tsai-Wu composites failure criteria, the safety factor contour is shown in Figure 5.3. As shown, the minimum safety factor is approximately 2.34, which was deemed sufficient. Lastly, the team has determined that the most relevant failure mode is fracture upon hard landing, as the various hatches on the fuselage skin may create stress concentrations. Therefore, the fuselage structure, along with the main landing gear and tail gear were modeled in ANSYS ACP for an explicit dynamics simulation on the hard landing scenario (Figure 5.4). The results show the stress distribution in the fuselage structure during free fall from a height of 2 ft. Maximum stress occurs at the intersection between the bottom fuselage skin and the landing gear, reaching 34,170 psi, which is safely below the ultimate strength.



Figure 5.1: Fuselage CAD.

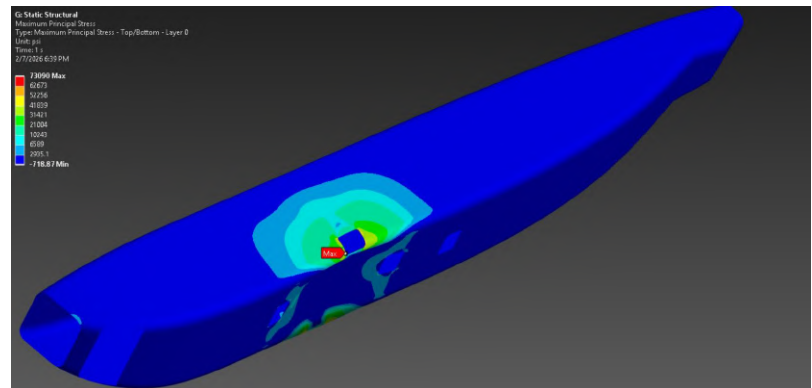


Figure 5.2: FEA simulation on fuselage from wing loads.

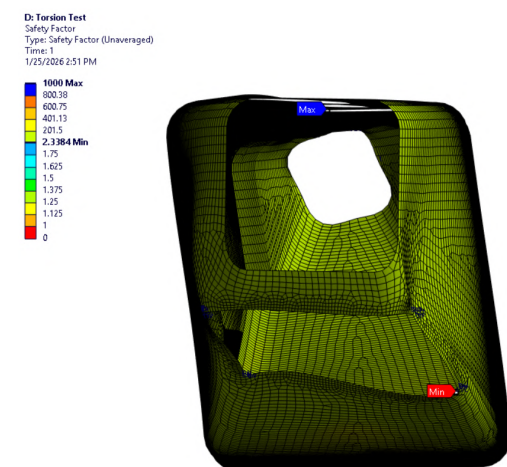


Figure 5.3: Torsional loading on fuselage.

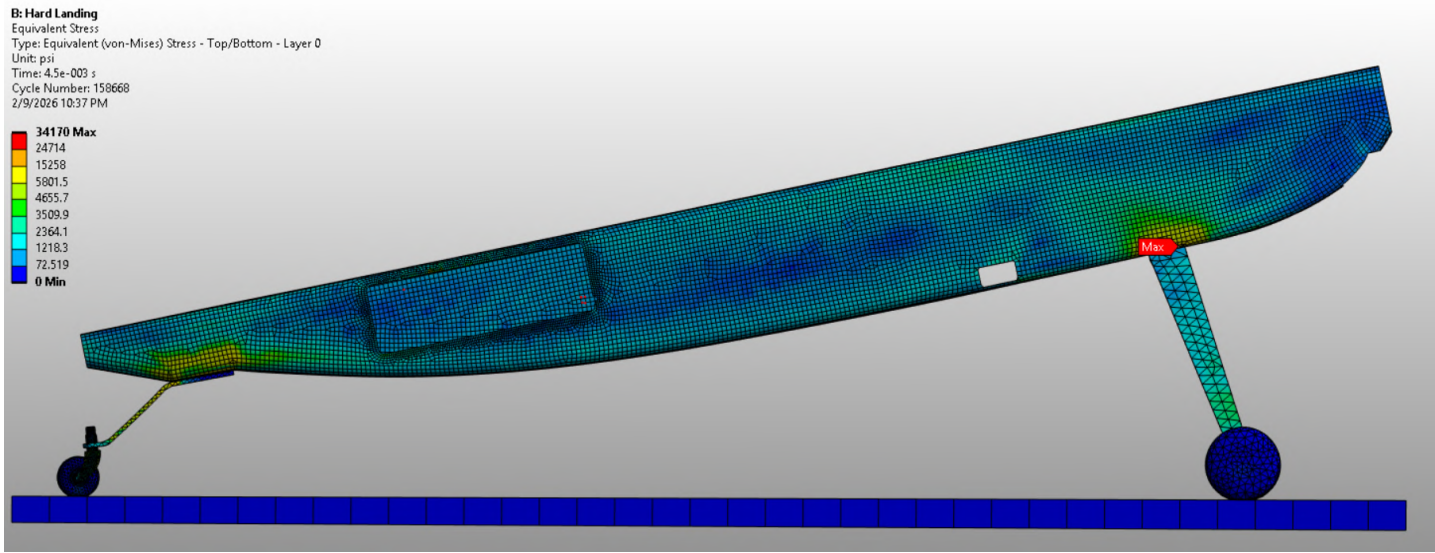


Figure 5.4: Hard landing simulation on the fuselage structure.

5.2.2 Wing

The wing design follows the NACA 4412 airfoil shape, chosen for its high lift-to-drag (L/D) at 4° angle of attack, common for cruising. The wingspan was sized to 59" to allow for manufacturing tolerances, and the chord length was sized to 10". The team has chosen not to minimize the wingspan because, as discussed in the sensitivity studies, a larger wingspan allows more laps to be completed and reduces the energy required for flight, which was critical for maximizing M2 and M3 scores. The wing was mounted in the lower fuselage section to allow easy payload access for M2 and GM. A rectangular 0.75" x 1.5" carbon fiber tube from Dragonplate [7] with a wall thickness of 0.0625" and 33 MSI fiber modulus, capable of withstanding up to 25 Gs of force with the full payload weight, runs through the middle 48" of the wing. The rectangular tube was chosen for its ability to prevent wing twisting. For ease of transportation, the team designed the wing in two halves that can be attached to the carbon fiber spar, which is constrained to allow only translation within a plywood wing mount (Figure 5.5). To fully secure the wing, M3 bolts running through the wing and the spar, along with locknuts, are used to secure the wing halves in place.

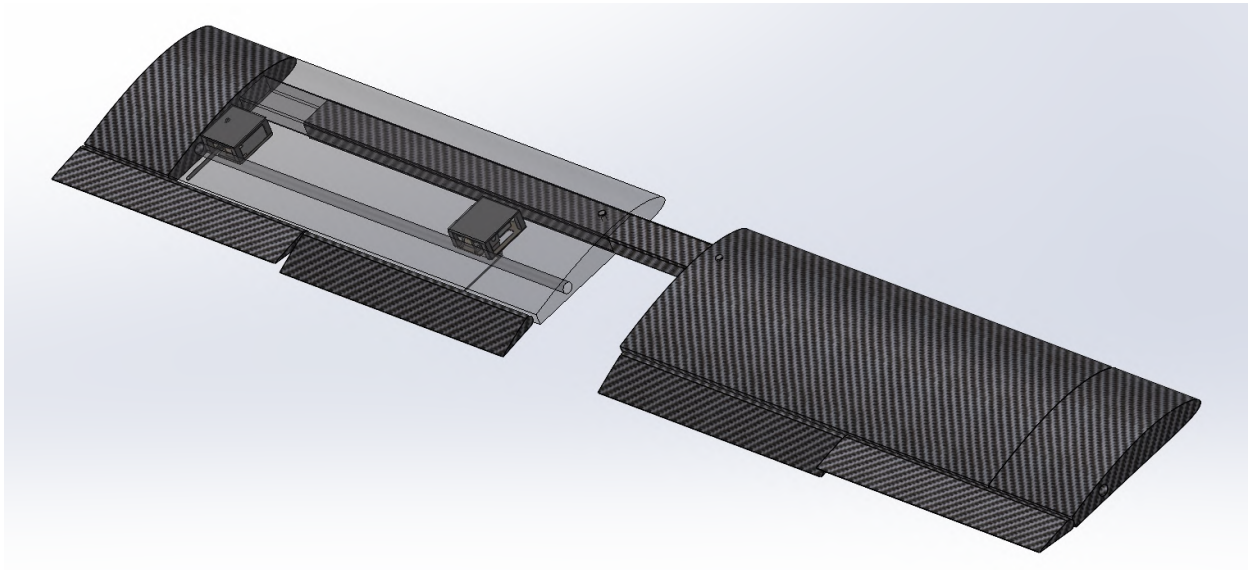


Figure 5.5: Wing assembly CAD.

The team performed an FEA simulation in Abaqus to assess torsional load on the wing (Figure 5.6), as the rectangular carbon fiber spar was deemed to provide more than enough bending stiffness. The model was constructed from three parts: a carbon fiber spar, an XPS foam core, and a $\pm 45^\circ$ bidirectional carbon fiber weave. The results indicate a very low shear stress of 755 psi.

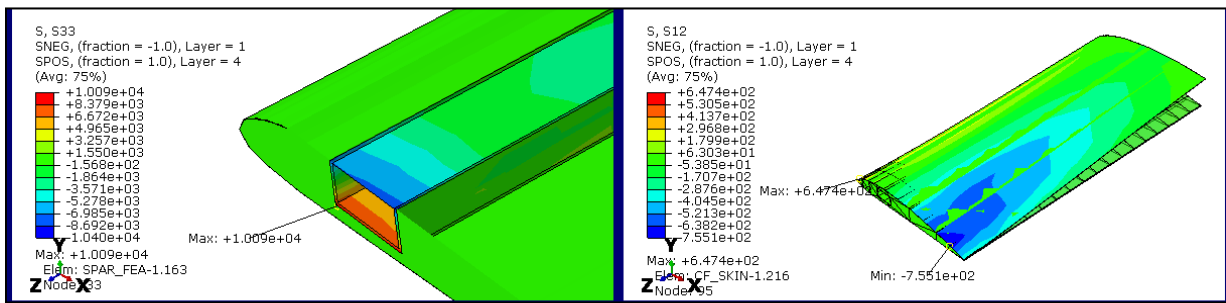


Figure 5.6: FEA simulation on torsional loading on wing.

5.2.3 Empennage

The span of the horizontal stabilizer is 20.94", and for the vertical stabilizer, it is 12.6". The NACA 0012 airfoil shape was selected for the stabilizers for its symmetry. A modular wooden support structure for joining empennage components (Figure 5.7) was constructed in three sections—one permanently attached to the vertical stabilizer, another to the horizontal stabilizer, and the last between two bulkheads in the fuselage. This structure serves as the primary attachment point for the empennage, allowing the tail assembly to be easily separated into individual components for transportation. The three sections are ultimately aligned and secured during assembly using two 0.25" diameter carbon fiber pins inserted orthogonally to the fuselage length. The complete assembly is shown in Figure 5.8.

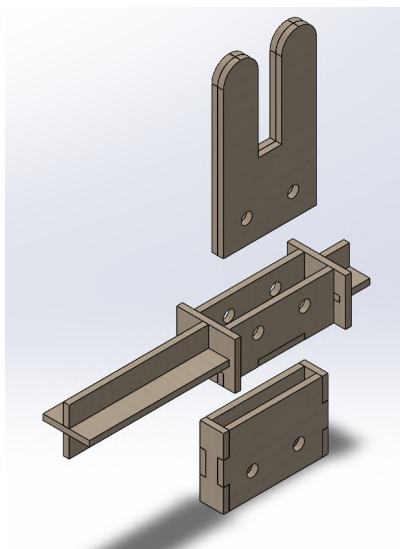


Figure 5.7: Tail-fuselage mount.

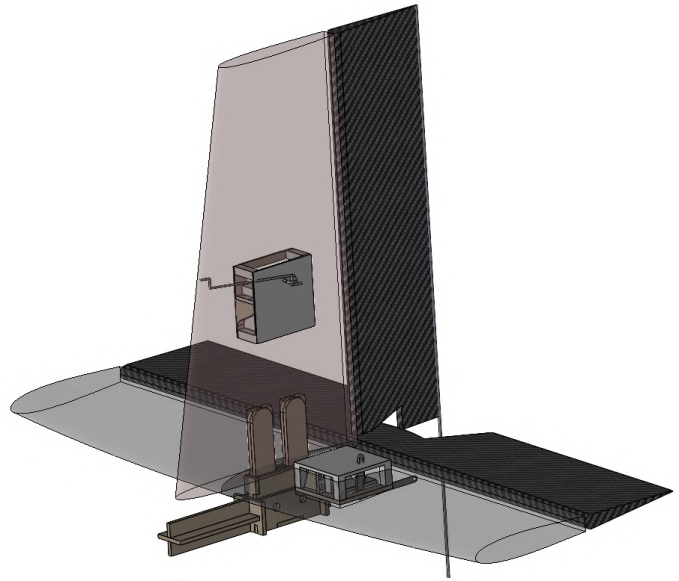


Figure 5.8: Tail assembly CAD.

A 1/8" diameter carbon fiber rod was epoxied to the trailing edge of the rudder (Figure 5.9). This rod extends beyond the span of the rudder all the way until it intersects with a rod hanging from the tail gear. This design allows the tail wheel to reorient and sync with rudder movement. This function has been proven influential on the team's aircraft in the previous DBF competition, as it allows steering during takeoff and after landing, eliminating the risk of running off the runway.

5.2.4 Landing Gear

The main landing gear and the tail gear were both constructed out of carbon fiber. The hard landing simulation results (Figure 5.10) extracted from the hard landing scenario indicate a maximum stress of 25,125 psi in the tail gear, which is safely below the ultimate strength.

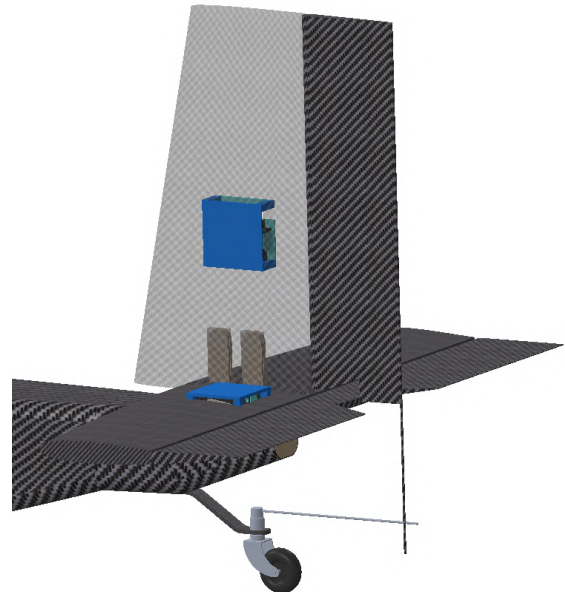


Figure 5.9: Rear-view of tail assembly.

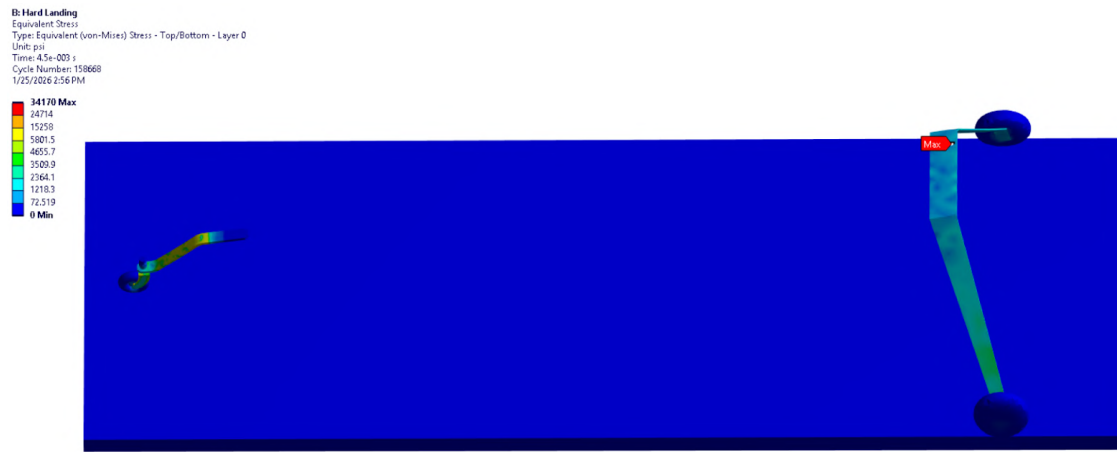


Figure 5.10: FEA simulation on landing gear.

5.2.4.1 Landing Gear Integration

As part of the design process, computational simulations were conducted to determine if wheel fairings are needed. Wheel fairings have been studied and concluded to reduce parasite drag by reducing the turbulence in the wake. A commercially available fairing was purchased and modeled in SolidWorks (Figure 5.11). Various simulations in ANSYS CFX [8] at the predicted M3 mission cruise speed were performed. It was found that with two added fairings, the total drag force produced by the landing gear assembly decreases from 0.344 lbf to 0.326 lbf, resulting in a total drag reduction of 0.018 lbf. The velocity contours (Figure 5.12) indicate flow circulation past the exposed wheel, whereas with the added wheel fairing, flow is more streamlined.

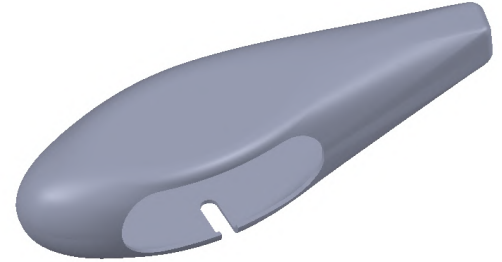


Figure 5.11: Wheel fairing CAD.

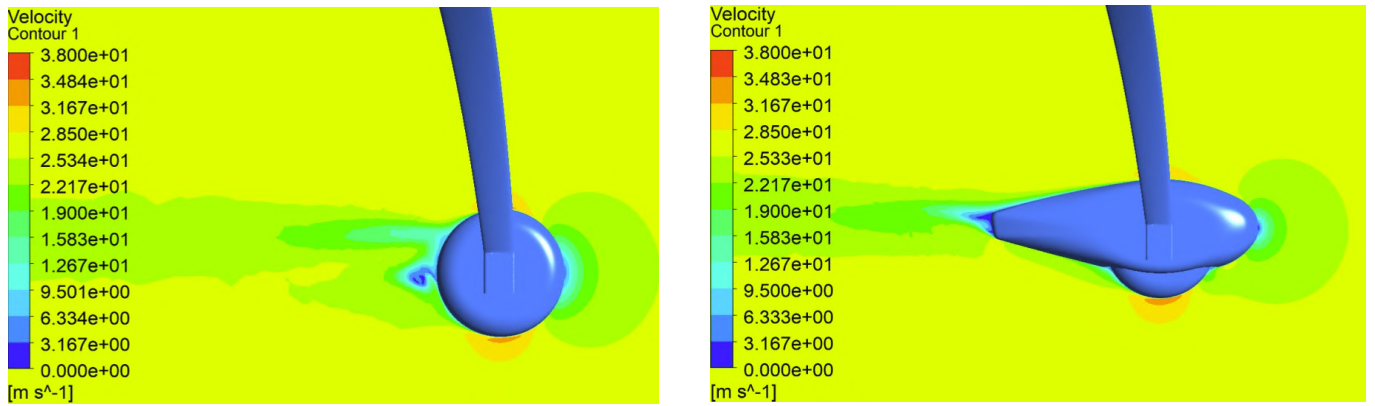


Figure 5.12: ANSYS CFD simulation on main landing gear with and without wheel fairing.

5.2.5 Passengers

Passengers are secured in the passenger compartment in "duck burgers" (also simply referred to as a "burger"). The duck burgers allow for quick, convenient loading and unloading of individual ducks, as well as restraining them in-flight to prevent translations and rotations. Inside the passenger compartment reside a "small burger" 9" long, and a "mega burger" 18" long. Both of these burgers are 4" wide and made from 1/16" basswood to fit within the tight space allotted for the passenger compartment. The burgers are attached to the floor by a rail system to easily guide batches of ducks farther into the fuselage without having the crew member insert his/her entire arm for each duck. This allows loading ducks into the passenger compartment only when the hatch is open, as once the burger is filled, it can be moved out of the way to make space for additional ducks.



Figure 5.13: Duck burger prototype.

The burgers consist of an elongated rectangular base with short walls on the long sides. Bass wood was chosen for the burger structure because it is low-density yet maintains the structural integrity needed to withstand movement during loading and in-flight turbulence. Restraining walls in the form of extensions to the side walls fold down to keep the ducks in place. The restraining walls are Velcroed closed to prevent them from releasing mid-flight. Egg crate foam is attached to the inside of the restraining walls to add additional support while accommodating the minor variations in duck shape and size.

The rail system consists of 3D-printed rails attached to the floor of the passenger compartment that span the full length, as well as 3D-printed rail "wheels" on the burgers that interlock with the floor rails. 3D-printed PLA was used due to its durability and ability to be formed into complex shapes. The hook-like shape of the rails prevents the burgers from lifting off the floor regardless of aircraft attitude.

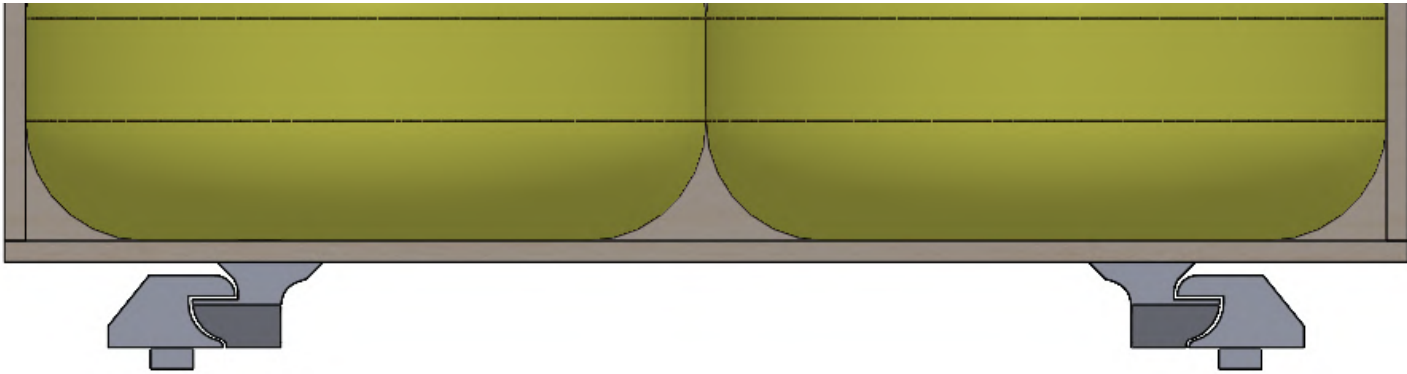


Figure 5.14: Burger rail system.

5.2.6 Cargo

The hockey puck storage container is a tray that can hold up to 8 hockey pucks in a line, with the pucks inserted from the top into holes in the tray. A 26" x 3.5" x 1" XPS foam board was hot-wire cut to include 8, 3" diameter holes to hold the hockey pucks. The foam tray has a bottom made from 1/16" thick balsa wood cut to go under the foam and support the weight of the pucks. To increase the bending stiffness of the balsa sheet, the team reinforced it with top and bottom carbon fiber cloths. This also makes the tray less prone to damage during handling and loading. The tray is designed to be loaded externally, then inserted through a door at the front of the plane, under the propeller, and slid into the fuselage. This cargo door is hinged to the fuselage surface. Inside the fuselage, openings in the bulkheads are laser-cut to include form-fitting holes to allow the tray to slide through. Additionally, guides are epoxied at the openings of the bulkheads to assist in aligning the tray with the hole.



Figure 5.15: Cargo holder CAD.

5.2.7 Banner

The complete CAD of the banner subsystem is presented in Figure 5.16. The banner is a 2' x 10' ripstop nylon fabric. The banner is stored on the flat region below the fuselage. A 1/8" diameter carbon fiber rod was attached to the leading edge of the banner. When the banner is stowed, one end is securely held by a 1/16" high tensile strength rope tied around a push rod belonging to the deploy servo. A small sphere is also hooked onto this side as a counterweight. The other end of the banner is secured by a 3D-printed cup made of PLA, with a drafted interior angle that allows the banner to slip out once the deploy servo on the other end releases the banner. The leading edge rod of the banner has a string running through it, forming a triangle with the end point looping around the push rod of the release servo.

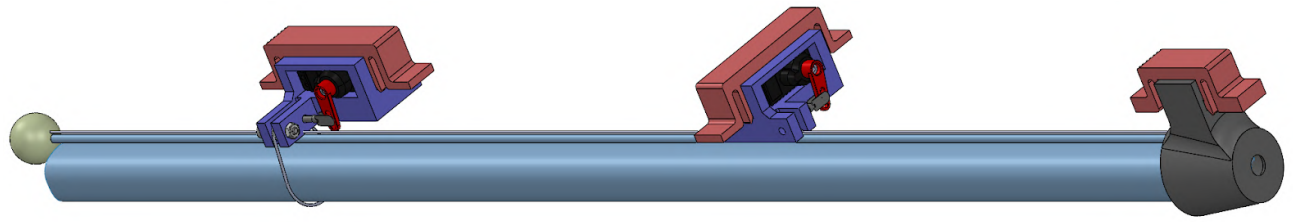


Figure 5.16: Banner subsystem assembly CAD (stowed configuration).

5.2.7.1 Banner Deploy Mechanism

The banner deploy mechanism consists of the forward-most servo and rear cup. The complete CAD of the banner deploy system is shown in Figure 5.17. A custom servo mount was designed in two configurations, one for the deploy servo and one for the release servo. The deploy servo is press-fit into the deploy servo mount, which includes two lug extensions that a push rod moves horizontally between. In the interior of the fuselage, a clamping structure is provided where the mount will be attached via snap fit. When it needs to be removed, the arms of the clamping structure can be pulled outwards to allow it to fall off. The distance between the two lugs is precisely such that a push rod fills the entire space when the servo arm moves to its extreme, and will be removed entirely from the space when the arm is at its other extreme. The servo arm is programmed not to move all the way to the right, as the push rod may fall out of the lug section and will need to be adjusted manually. A socket screw is secured parallel to the pushrod with a nut on the other side. A short high-strength rope is tied to two aluminum washers (one on each side), with one washer sitting on the socket screw and the other slotted onto the pushrod after wrapping over the banner. As the push rod moves out of the lug region, the washer falls off, and the rope follows, causing the front end of the furled banner to swirl downwards. This rotation motion causes the other end of the banner to slip out of the cup structure. After this deployment, the banner is towed kite-like, with the spherical weight keeping it upright.

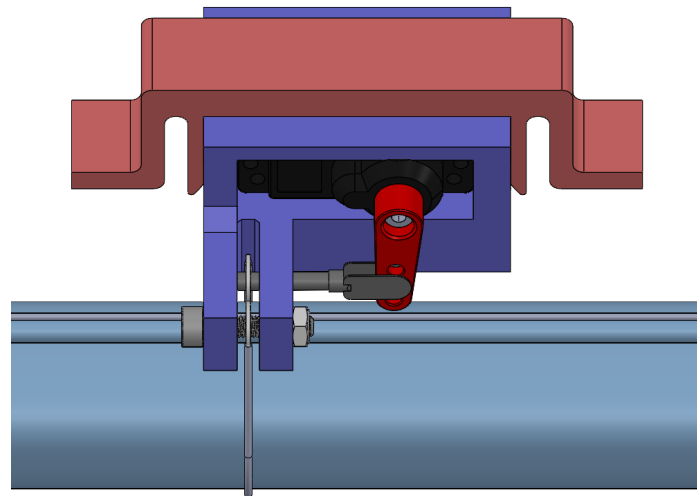


Figure 5.17: Banner deploy mechanism assembly.

5.2.7.2 Banner Release Mechanism

For the banner release mechanism (Figure 5.18), a similar mount structure as the one above for the deployment mechanism was used, the only change being the removal of the socket screw. The same snap-fit clamping structure is used to attach the mount to the fuselage interior. Note that both the deploy and release servo structures are located under the hockey puck tray. The rigging string that ends at the triangular junction is tied to a washer at its end. The washer is attached to a push rod that extends from a coupler on a servo arm. Since the pushrod is the sole attachment point of the rigging string after the banner is deployed, the banner and rigging string fall when the pushrod moves out of the lug space.

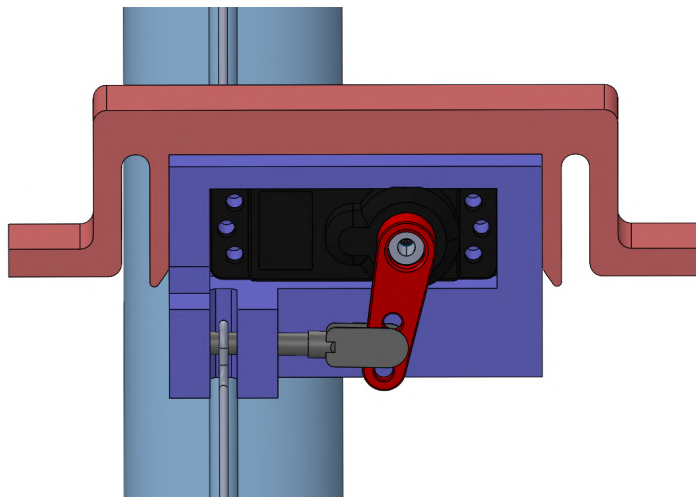


Figure 5.18: Banner release mechanism assembly.

5.2.8 Servo Mounts

Two types of servos for non-payload-related operations are used on the aircraft: the D-645MW and the HS-7245MH. The D-645MW is used for flaps, while the HS-7345MH is used for ailerons, rudder, and elevator. The HS-7245 features a metal geartrain that delivers high torque in a small package, which is crucial for critical control surfaces such as ailerons, rudder, and elevator. The mounts are 3-D printed and modular, allowing for servo maintenance between flights. A mount is designed with four legs, each containing a heat-set insert. Four of these mounts are permanently epoxied into the wing (two for ailerons, two for flaps), one is attached to the horizontal stabilizer, and the last is attached to the vertical stabilizer. They are placed such that the servo arm is at the halfway point for each control surface. The platform the servo is attached to has four holes matching these legs and two upright pieces with four heat-set inserts, matching the mounting holes on each servo. The servo with the platform can then be secured to the mount with four more M3 bolts. The sizing of the platforms and mounts is minimized to prevent collisions with the spar and wiring channels, while still being large enough to encompass the servo itself.

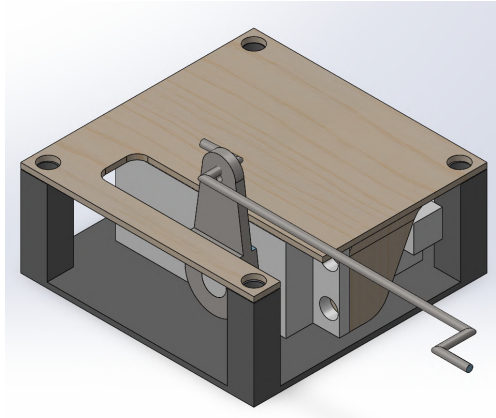


Figure 5.19: Servo mount assembly.

5.2.9 Avionics

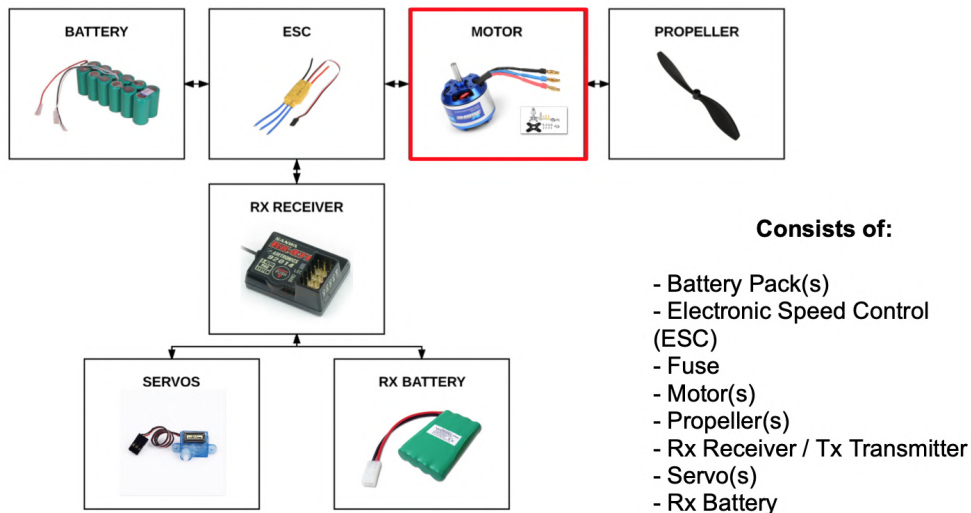


Figure 5.20: Flight avionics structure.

Figure 5.20 presents the structure of the flight avionics. A 4500 mAh LiPo (Lithium-ion-Polymer) battery with 6 cells was chosen to meet as much of the 100 Wh competition requirement as possible. The ESC was mounted on the top surface of the fuselage such that the heat sink would be exposed to incoming airflow during flight. Antennas were placed on the top and bottom of the fuselage surfaces to eliminate the possibility of losing signal due to the conducting nature of carbon fiber.

5.3 Weight and Balance

The weight-and-balance data for each flight configuration are shown in Table 5.2. X-position measures the relative position with respect to the frontal surface of the fuselage. Due to the high length of the passenger and cargo restraint system, they were designed to be positioned so that their combined CG would balance at

around 25% chord past the wing's leading edge. Note that the motor and propeller have a negative x-position value, as they are located before the nose of the fuselage.

Table 5.2: Weight and balance data for flight configuration.

| Component | X-Position (in) | Mass (lb) | | |
|---------------------------------------|-----------------|-----------|-------|-------|
| | | M1 | M2 | M3 |
| Fuselage | 25.12 | 2.16 | 2.16 | 2.16 |
| Wing | 18.61 | 2.33 | 2.33 | 2.33 |
| Horizontal Stabilizer | 56.43 | 0.51 | 0.51 | 0.51 |
| Vertical Stabilizer | 55.62 | 0.52 | 0.52 | 0.52 |
| Landing gear (main) | 9.70 | 0.71 | 0.71 | 0.71 |
| Landing gear (tail) | 54.62 | 0.10 | 0.10 | 0.10 |
| Passengers + Restraint Systems | 26.83 | 0.16 | 1.46 | 0.16 |
| Cargo + Restraint System | 16.36 | 0.3 | 3.17 | 0.3 |
| Banner + Deploy/Release System | 18.84 | 0.16 | 0.74 | 0.74 |
| Battery | 3.80 | 1.47 | 1.47 | 1.47 |
| ESC | 4.34 | 0.33 | 0.33 | 0.33 |
| Avionics Battery | 5.88 | 0.30 | 0.30 | 0.30 |
| Motor + Propeller | -1.78 | 1.43 | 1.43 | 1.43 |
| Additional Electronics | - | 0.25 | 0.25 | 0.25 |
| Miscellaneous | - | 0.04 | 0.04 | 0.04 |
| Total Mass (lb) | | 10.74 | 15.53 | 11.32 |
| CG Location | | 18.18 | 18.29 | 18.11 |

5.4 Flight Performance

The aircraft's performance is affected by its aerodynamic characteristics, propulsion efficiency, and structural integrity. Key flight performance parameters include lift-to-drag ratio, stall speed, maximum cruise speed, rate of climb, and turn radius.

The aircraft uses the NACA 4412 airfoil, chosen for its high C_L/C_D ratio over a range of angles of attack and progressive stall characteristics. At a cruise angle of attack of 2 degrees, the aircraft generates sufficient lift to support its design payload while maintaining low drag. The maximum lift coefficient is estimated to be 1.4, ensuring safe operation at low speeds.

The stall speed is approximately 35 ft/s, calculated based on the aircraft's maximum takeoff weight and wing loading. For M1, the team will complete 3 laps in under two minutes, with a top flight speed of 97 ft/s.

Adding 4.8 lb of payload for M2 (24 rubber ducks and 8 hockey pucks), the team will complete 7 laps in the five-minute time window with a top speed of 92 ft/s. During M3, the team will have a banner sized 2 x 10 ft while executing 5 laps in the five-minute time window, with a top speed of 84.1 ft/s.

The aircraft's rate of climb is estimated at 20 ft/s at full throttle. This is achieved by pairing the Scorpion A-5025-415kv motor with an APC 18x12E [9] propeller to account for lower cruise speeds due to banner drag. The propulsion system is optimized for both takeoff acceleration and sustained cruise efficiency. The turn radius is minimized to maximize the number of laps in Mission 3 while ensuring structural integrity under a 4g load factor at a 75-degree bank angle.

Drag contributions from the fuselage, wing, payload, and landing gear were analyzed, revealing that parasitic drag dominates at competition flight speeds. Selecting streamlined components and optimizing payload placement reduces overall drag and enhances aerodynamic efficiency. Flight tests and wind-tunnel measurements will validate these theoretical predictions, enabling further refinements.

5.5 Mission Performance

The aircraft's mission performance is evaluated based on its ability to successfully complete each competition task while optimizing for speed, payload capacity, and autonomous operations.

In M1 (Test Flight), the aircraft is designed for a stable, controlled takeoff and landing while carrying the required payload.

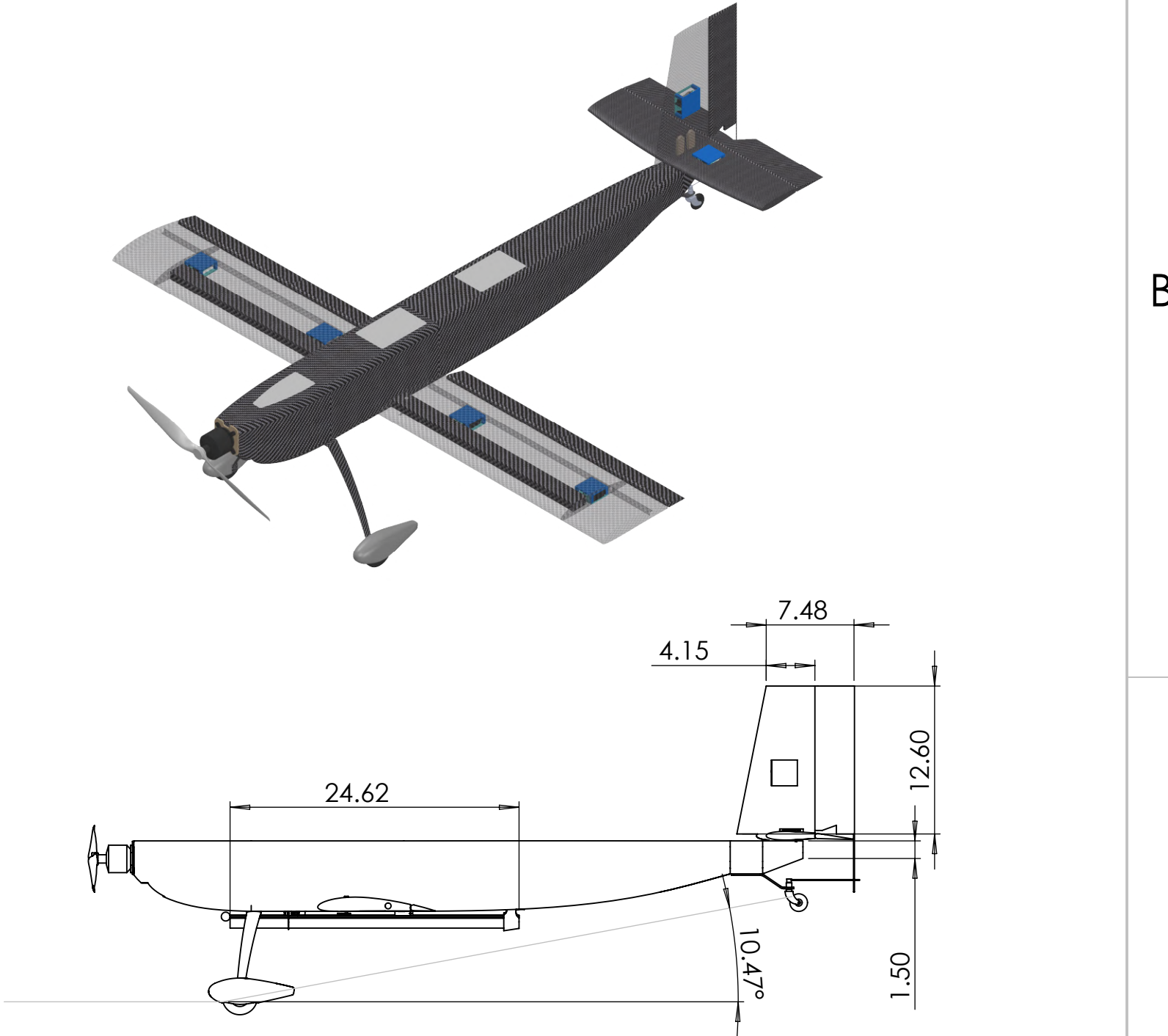
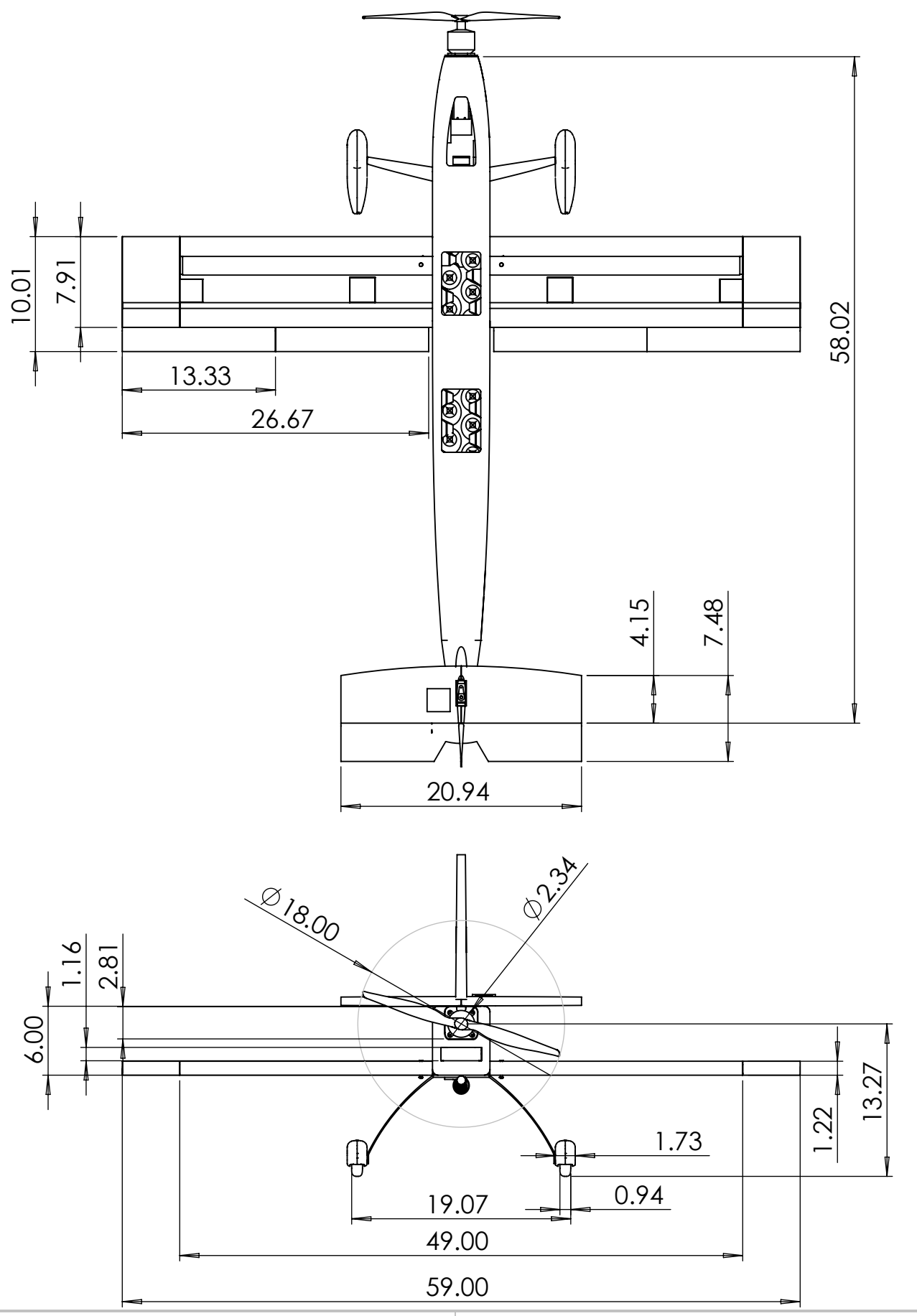
For M2, the primary objective is to maximize payload weight while maintaining a cruise speed of 92 ft/s. Twenty-four rubber ducks will be housed in the fuselage, along with 8 hockey pucks in the cargo compartment directly underneath, for a total payload of 4.8 lb. The aircraft completes seven laps within the five-minute window, maintaining structural integrity under the additional load. The optimized wing structure with a carbon fiber spar ensures minimal flexing under these conditions. This results in an estimated net income of 742.

M3 requires the aircraft to deploy and release the banner, all while maximizing the number of laps completed. The team will use a banner measuring 2 x 10 ft to maximize score while minimizing banner-induced drag during 5 laps within the five-minute time window. This results in an estimated unnormalized score of 286.

GM requires the aircraft to be configured quickly within a five-minute staging window. The payload loading mechanisms, battery installation, and servo mounting were designed for rapid deployment. Testing will ensure that all components can be assembled efficiently under competition constraints. Preliminary tests of GM estimate a time of 90 seconds.

Overall, the aircraft's design and performance parameters align with mission objectives, emphasizing aerodynamic efficiency, structural robustness, and effective mission execution. The team's iterative testing and refinement process will further optimize these aspects, ensuring competitive success.

5.6 Drawing Packages



| | | |
|---------------------------------------------------------|-----------|--------------------------|
| | NAME | Peaking Jay |
| DRAWN BY | Han Zheng | Johns Hopkins University |
| All dimensions are in inches unless otherwise specified | | |
| Aircraft 3-View | | REV |
| SCALE: 1:12 | | SHEET 1 OF 4 |

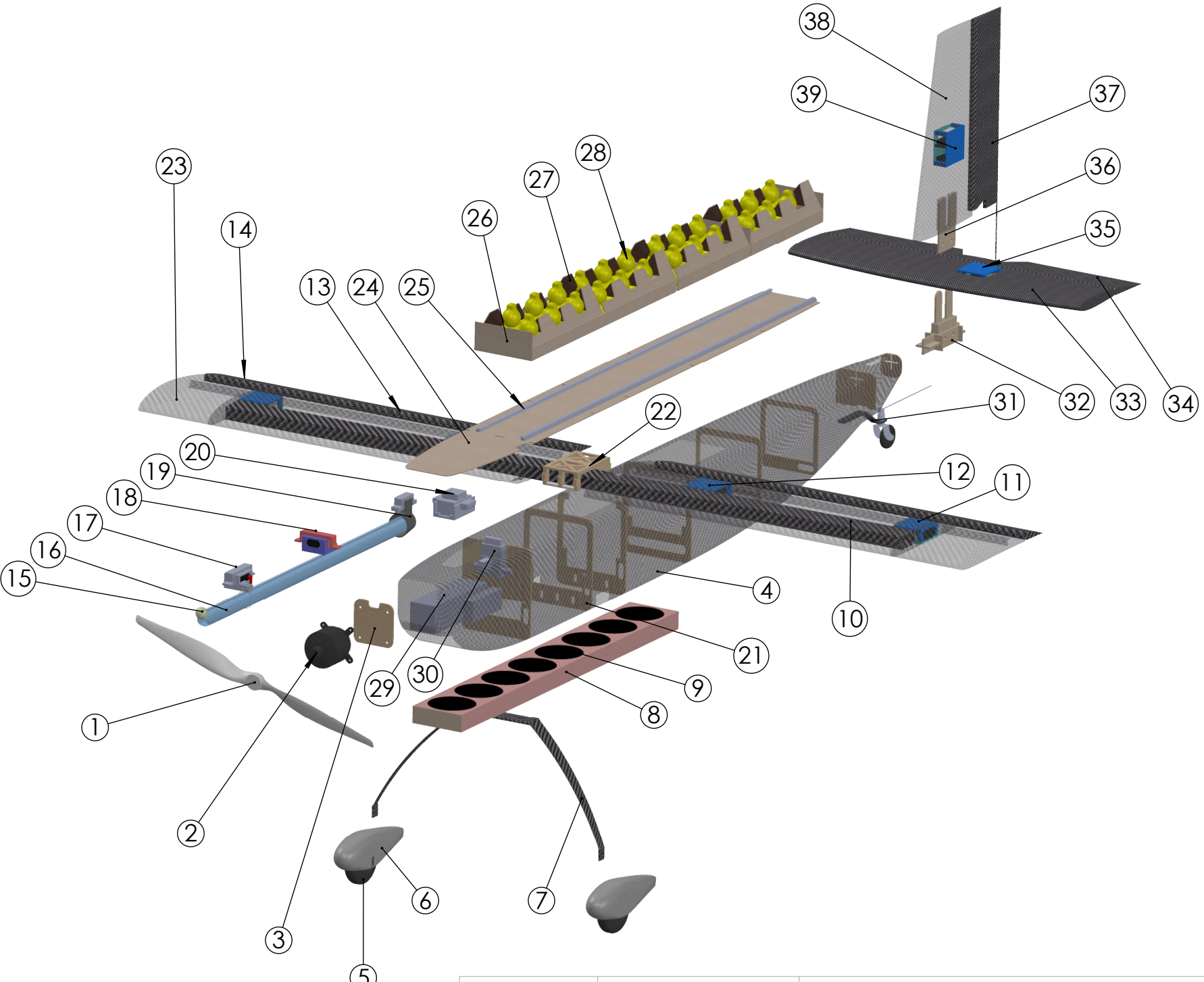
4

3

2

1

| ITEM NO. | PART NAME | Description |
|----------|------------------------------|--------------------------|
| 1 | Propeller | Glass-Reinforced Plastic |
| 2 | Motor | Scorpion A-5025-215kV |
| 3 | Motor Bulkhead | Plywood |
| 4 | Fuselage Skin | Carbon Fiber |
| 5 | Front Landing Gear Wheel | Rubber |
| 6 | Wheel Fairing | Fiberglass |
| 7 | Front Landing Gear | Carbon Fiber |
| 8 | Cargo Holder | XPS Foam |
| 9 | Cargo (Hockey Puck) | Rubber |
| 10 | Wing Spar | Carbon Fiber |
| 11 | Aileron Servo | HiTec HS-7245MW |
| 12 | Flap Servo | HiTec D645MW |
| 13 | Flap | Carbon Fiber/XPS Foam |
| 14 | Aileron | Carbon Fiber/XPS Foam |
| 15 | Banner Leading Edge Weight | PLA |
| 16 | Banner | Ripstop Nylon |
| 17 | Banner Deploy Mechanism | PLA |
| 18 | Banner Release Mechanism | PLA |
| 19 | Banner Rear Holder | PLA |
| 20 | ESC | Scorpion Tribunus III |
| 21 | Bulkhead | Plywood |
| 22 | Wing Spar Mount | Plywood/PLA |
| 23 | Wing Skin | Carbon Fiber |
| 24 | Floor | Basswood |
| 25 | Floor Rails | PLA |
| 26 | Passenger Restraint System | Basswood |
| 27 | Foam Block | Polyurethane |
| 28 | Passenger (Rubber Duck) | Rubber |
| 29 | Battery | Roaring Top 6s 4500 mAh |
| 30 | Fuse | 100AMP Fuse |
| 31 | Tail Gear | Carbon Fiber |
| 32 | Horizontal Stabilizer Insert | Plywood |
| 33 | Horizontal Stabilizer | Carbon fiber/XPS Foam |
| 34 | Elevator | Carbon Fiber/XPS Foam |
| 35 | Elevator Servo | HiTec HS-7245MW |
| 36 | Vertical Stabilizer Insert | Plywood |
| 37 | Rudder | Carbon Fiber/XPS Foam |
| 38 | Vertical Stabilizer | Carbon Fiber/XPS Foam |
| 39 | Rudder Servo | HiTec D645MW |



| | | |
|---------------------------------------------------------|--------------|--------------------------|
| | NAME | Peaking Jay |
| DRAWN BY | Han Zheng | Johns Hopkins University |
| All dimensions are in inches unless otherwise specified | | |
| Exploded View | | |
| REV | | |
| SCALE: 1:8 | SHEET 2 OF 3 | |

4

3

2

1

4

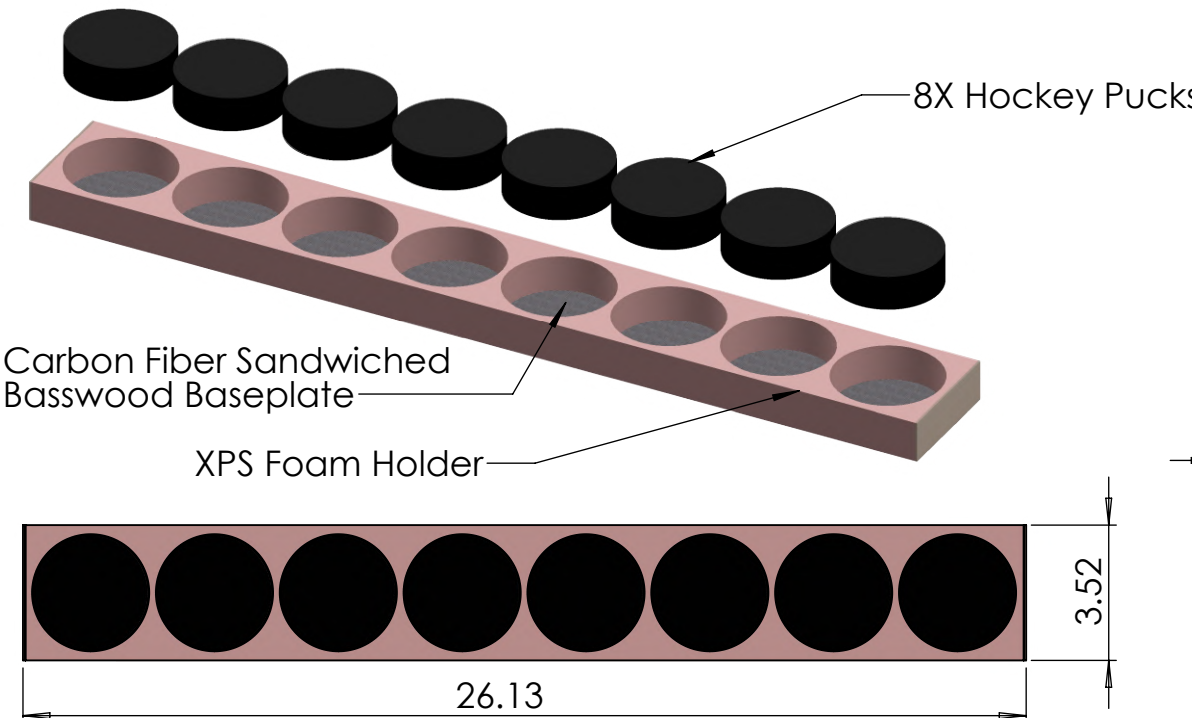
3

2

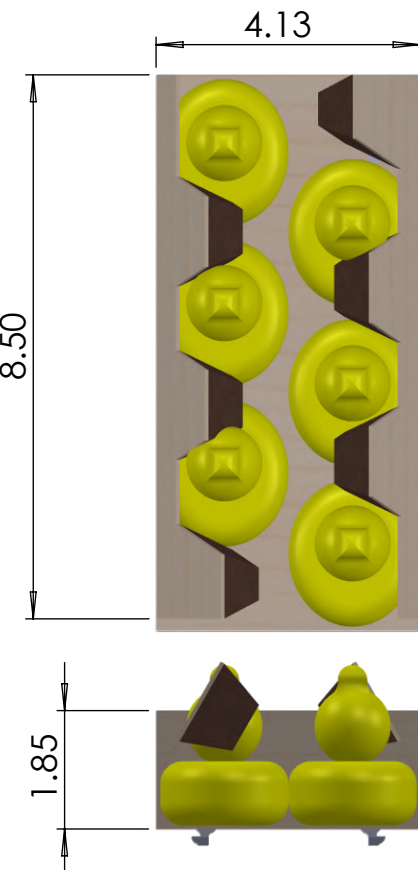
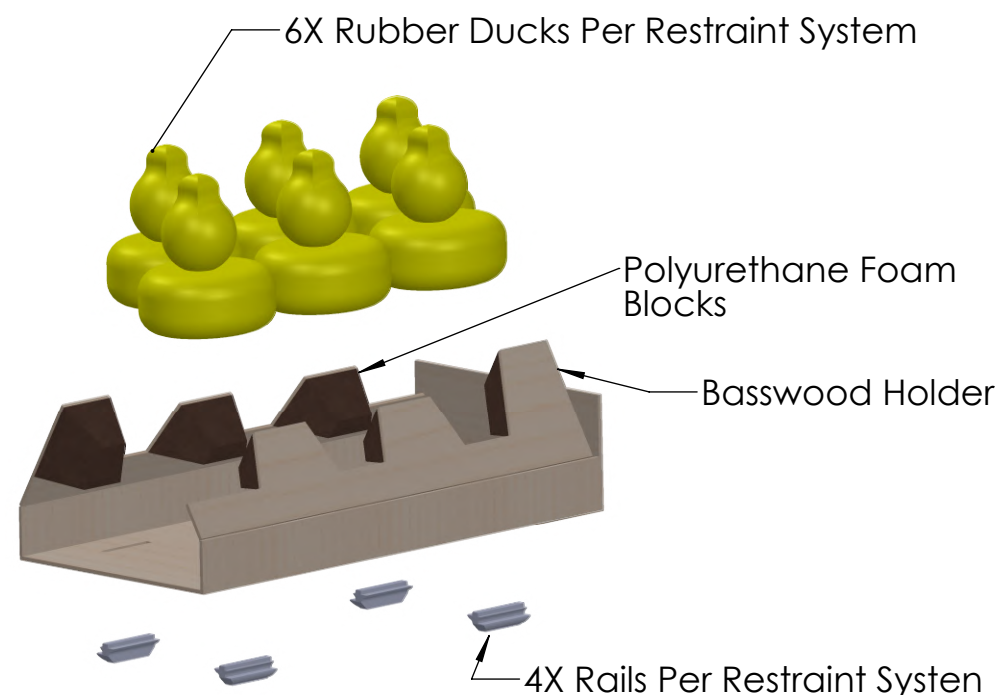
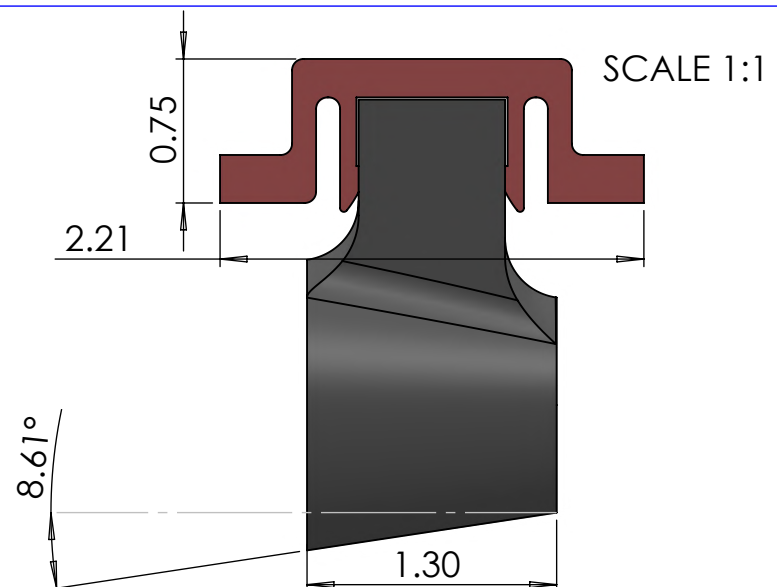
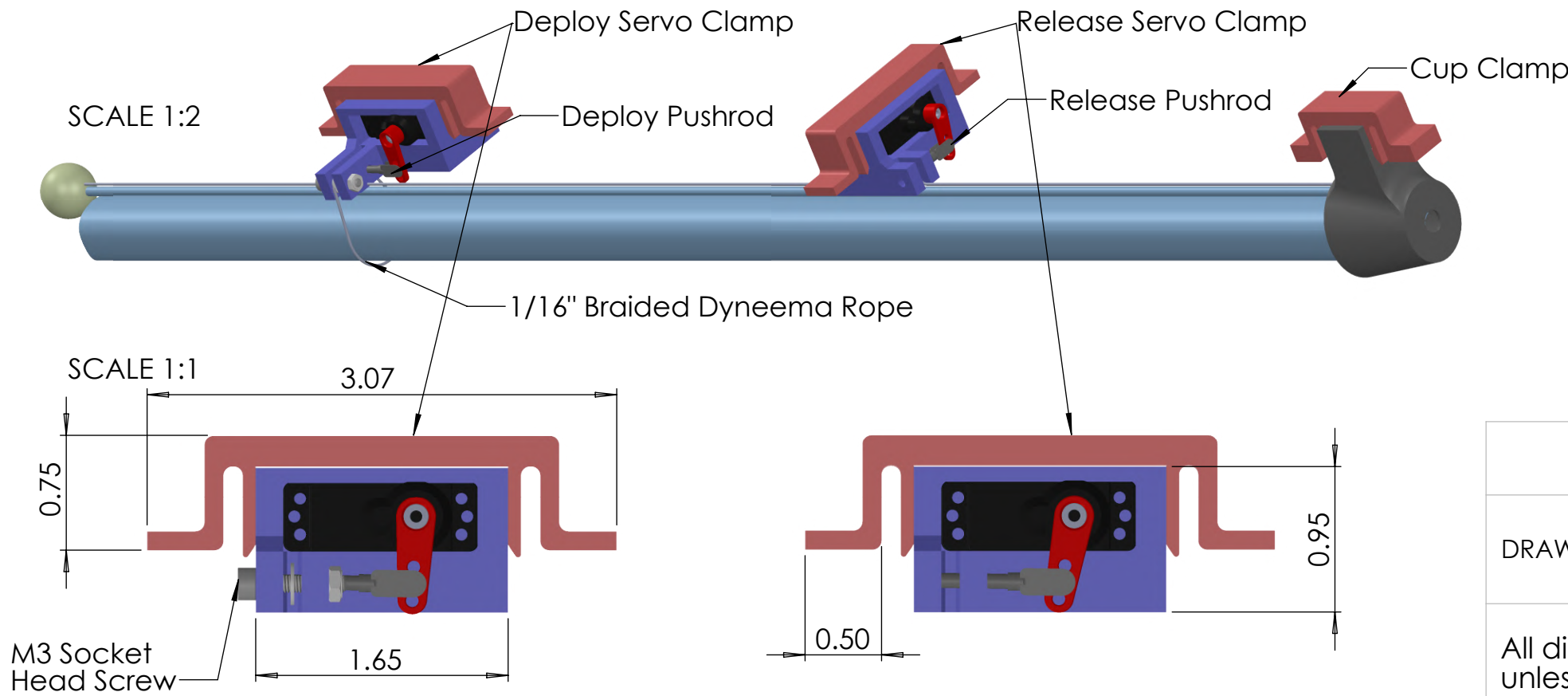
1

CARGO RESTRAINT SYSTEM ASSEMBLY

SCALE 1:5

**PASSENGER RESTRAINT SYSTEM ASSEMBLY**

SCALE 1:3

**BANNER ASSEMBLY**

| | | |
|---------------------------------------------------------|-----------|--------------------------|
| | NAME | Peaking Jay |
| DRAWN BY | Han Zheng | Johns Hopkins University |
| All dimensions are in inches unless otherwise specified | | |

REV

SHEET 3 OF 3

4

3

2

1

6. Manufacturing Plan

6.1 Manufacturing Process:

6.1.1 Additive Manufacturing (3D Printing)

Additive manufacturing, specifically 3D printing, can be used to prototype parts to assess design validity. It is an optimal method to manufacture fixtures for avionics components and onboard mechanisms. It can often be used to manufacture parts with small, complex geometries or to fabricate molds. The team has access to the university's Bambu Lab X1 Carbon FDM printers and PLA filaments.

6.1.2 Laser Cutting

Laser cutting is commonly used to cut or engrave wood or acrylic. It can be used to produce parts with uniform thickness and complex 2D geometry with high accuracy. This method enables rapid prototyping of wood components to verify tolerances and produce parts with different geometries.

6.1.3 CNC Hotwire Cutting

The team has a custom-made CNC hotwire cutter (Figure 6.1) from previous competition history. It is a subtractive manufacturing method that uses a heated Nichrome wire to carve out of an XPS foam block. It is an optimal method for making an XPS foam mold. However, depending on the wire feed rate, current, and other parameters, the finished product might have poor tolerances.

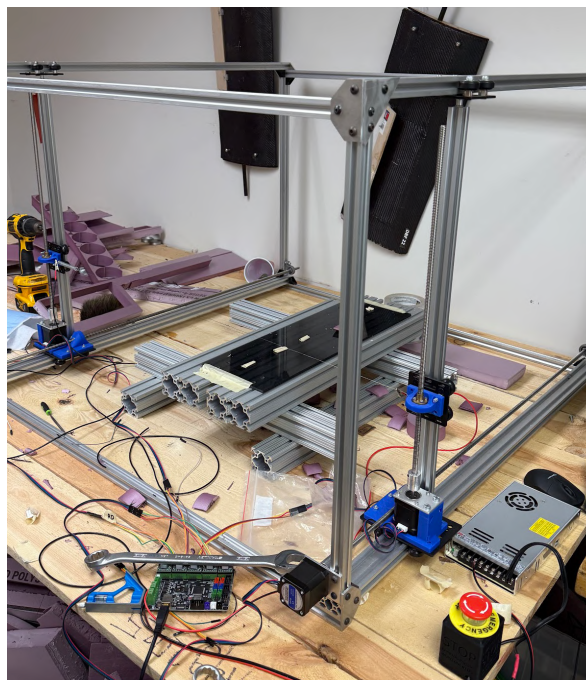


Figure 6.1: JHU hot wire cutter.

6.1.4 Carbon Fiber Layup

Carbon fiber layup is a fundamental composite manufacturing technique that enables the production of complex geometries. With a well-treated mold, multiple layers of carbon fiber cloth can be laid up at custom angles to achieve the desired stiffness in various directions. Specifically, wet layups with room-temperature cure are chosen for their lower cost. The mold, carbon fiber cloths, peel plies, and breather cloths are placed inside a vacuum bag, which is then connected to a vacuum pump to ensure the material conforms to the mold surface.

6.1.5 Manual and CNC Machining

Manual machining is a subtractive manufacturing technique commonly used to process metals. Due to their high density, metals are rarely used on DBF aircraft, unless specific components require high compressive strength. Computer numerical control (CNC) machining, on the other hand, can produce parts with complex geometries up to 6 degrees of freedom. It involves using pre-programmed software to control machine tools that cut materials precisely, removing material from a block to create a finished part. It can be used to manufacture a mold from XPS foam blocks with high accuracy, provided that appropriate spindle speed, feed rate, and plunge rate are inputted.

6.2 Manufacturing Process:

6.2.1 Fuselage

A 1:3 scale model of the fuselage was first manufactured and assembled to test the carbon fiber wet layup process planned for the full fuselage assembly. 3D printed female molds were used for this model. The actual fuselage was manufactured in top and bottom halves, using the same wet layup method as for the scale model. For the full-scale model, the female molds were manufactured by CNC milling multiple stacked XPS foam blocks. Surface bulges were designed on the molds to mark precise positions of access doors that would be dremeled later in the process. Slow-cure epoxy was applied to the mold surface to fill porosities. Multiple sanding iterations were performed to ensure the mold surface was smooth enough to achieve a satisfactory finish. Polyvinyl alcohol (PVA) was applied multiple times to allow for easy separation between the mold and carbon fiber parts. Three 2x2 twill weave bidirectional carbon fiber cloths were applied in 0/90, ±45, and 0/90 degrees. Peel plies and breather cloths were placed on the interior surfaces to absorb excess epoxy. The two halves were placed in a vacuum bag with the vacuum pump operating for 12 hours, then left to cure at room temperature for another 12 hours. The edges of the cured parts were dremeled and sanded later. Additionally, the fuselage access openings were dremeled and sanded with a sanding drum. Figure 6.2 shows the top half of the fuselage during the vacuum bagging process and finished part after a 24-hour cure. The two halves

have a 1/2" overlapping lip region where one half can slide into the other. The two halves were then joined using bolted joints along the overlapping lip.



Figure 6.2: Vacuum bagged fuselage (left) and cured fuselage (right).

6.2.2 Wing

The wing was constructed by laying up carbon fiber on an XPS foam core (Figure 6.3). A profile of the wing, along with the channels for a commercially sourced 0.86" x 1.60" x 48.50" structural carbon fiber tube and wiring, was cut out of a block of XPS foam using the CNC hot wire cutter. In addition to separating the port and starboard wings, each half of the wing was further separated into two sections to facilitate cutting and to account for different cross sections as a result of aileron, flap, and carbon fiber tube length, which does not extend the entire wing span. The four finished sections were then assembled with the carbon fiber tube in place to provide structural support during vacuum bagging. During this process, the decision was made to wrap the carbon fiber tube in three layers of PVA film to allow the tube to be separated from the two halves of the wing upon completion. A single layer of carbon fiber cloth with epoxy resin was applied to the XPS foam core, along with associated peel plies and breather cloths, and then placed in a continuously running vacuum bag for 12 hours to dry. Finally, the assembly was removed from the bag, and the peel plies and breather cloth were removed to reveal the finished wing assembly.

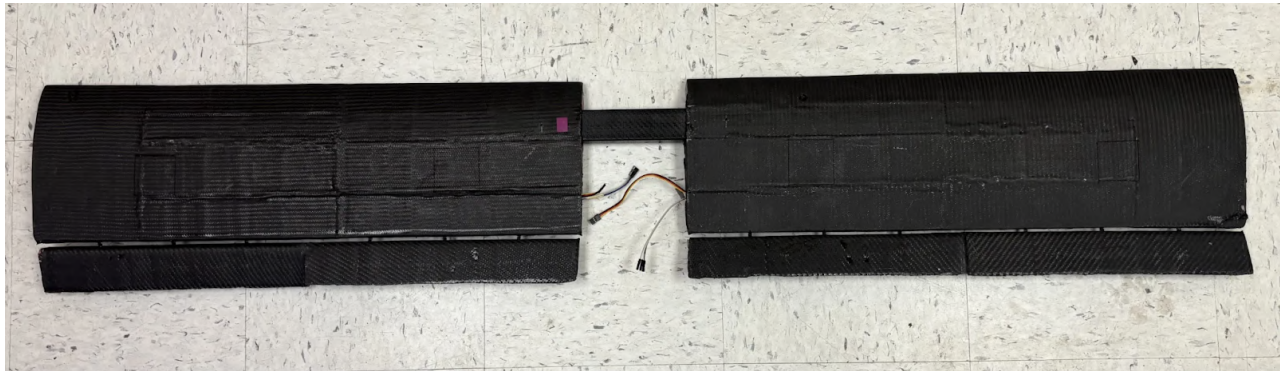


Figure 6.3: Both halves of the wing assembled to the carbon fiber spar.

6.2.3 Empennage

The empennage was constructed using XPS foam, carbon fiber, balsa wood, wood glue, and epoxy resin (Figure 6.4). Foam cores with the shape of vertical and horizontal stabilizers were cut and separated from a block of XPS foam using the CNC hot wire cutter. Separately, the pieces that comprised the empennage “anchor” were laser cut from a sheet of $\frac{1}{8}$ ” plywood and glued together with wood glue. A single layer of carbon fiber was laid onto the XPS foam with epoxy, followed by peel plies and breather cloth, and then placed in a vacuum bag for 12 hours to dry. After drying, the peel plies were removed along with the breather cloths, and negative spaces were carved into the vertical and horizontal stabilizers to facilitate assembly with the empennage anchor. Finally, the anchor, along with the stabilizers were assembled with epoxy resin and dried.



Figure 6.4: Empennage assembly.

6.2.4 Control Surfaces

The control surfaces, including the ailerons, flaps, rudder, and elevator, were also constructed using XPS foam, carbon fiber, and epoxy resin. Foam cores with the shape of each control surface were cut and extracted from a block of XPS foam measuring 0.5" thick using the CNC hot wire cutter. A single layer of carbon fiber was laid onto the XPS foam with epoxy, followed by peel plies and breather cloth, and then placed in a vacuum bag for 12 hours to dry. After drying, the peel plies and breather cloths were removed. For the ailerons, flaps, and rudder, three holes are drilled at the leading edge center and spaced equidistantly from one another, while the elevator has four holes drilled at the leading edge. Plastic hinges were then epoxied into these holes.

6.2.5 Landing Gear

Both the main landing gear and the tail gear were purchased because their dimensions met the aircraft's design requirements. Four holes were drilled manually on the surface of the main landing gear to allow for attachment to the fuselage. One hole on each side of the main gear was also drilled to allow attachment of axles and wheels. Wheel fairings were dremoled to provide sufficient clearance from the wheels and epoxied to the main gear. Three holes were drilled in the tail gear and fuselage to allow for attachment to the rear part of the fuselage.

6.2.6 Passenger and Cargo Restraint System

Figure 6.5 shows the complete assembly of one "burger." The "burger" primarily consists of 1/16" laser-cut basswood. The basswood pieces were held together by wood glue, and egg-crate foam was cut into small pieces and glued to the jigsaw-shaped side walls. Two pieces of Velcro were attached to the side walls to help keep passengers in place. Rails that are 3D printed in PLA are attached to the bottom basswood piece, allowing the restraint system to slide on the floor inside the fuselage.



Figure 6.5: "Burger" assembly with the passengers secured.

The cargo holder is a rectangular block with patterned holes to house hockey pucks (Figure 6.6). It was first cut from an XPS foam block using a hot-wire cutter to provide the circular constraint spaces. One 1/16" basswood sheet was sandwiched with one layer of carbon fiber on both sides to provide stiffness. The balsa sheet was then epoxied to the XPS foam structure to serve as the base plate. Iterations of sanding were performed on the carbon fiber-sandwiched balsa sheet, and masking tape was applied to create smooth edges, which would assist with the loading and unloading process.

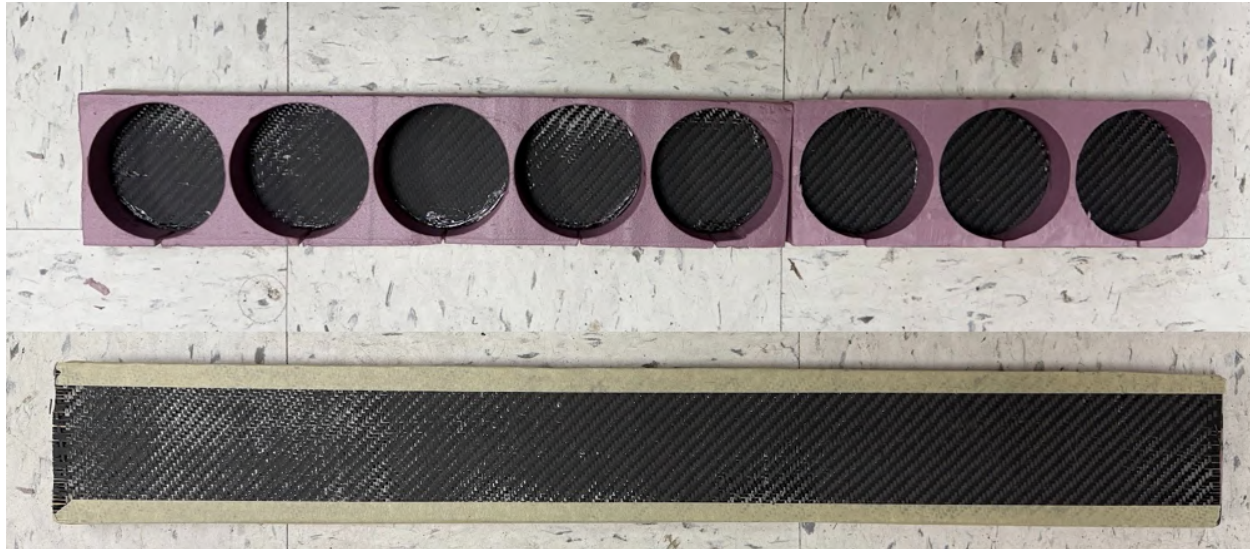


Figure 6.6: Cargo holder (top and bottom view).

6.2.7 Banner Deploy and Release Mechanism

The banner deploy and release mechanisms were 3D-printed (Figure 6.7). It allows rapid prototyping, enabling repeated testing and changes, provides reasonable strength, and is lightweight at the same time. Iterations of test prints have been done to test the snap-fit mechanism between the clamping structure and the banner servo mounts. It was concluded that an infill density of 15% is best suited for the clamping structure, and for the banner servo mount it is 10% in order to minimize weight. Aluminum M3 socket screws were secured to the lugs via bolted joints. A threaded rod was screwed into the pushrod of the servo to allow for linear actuation.

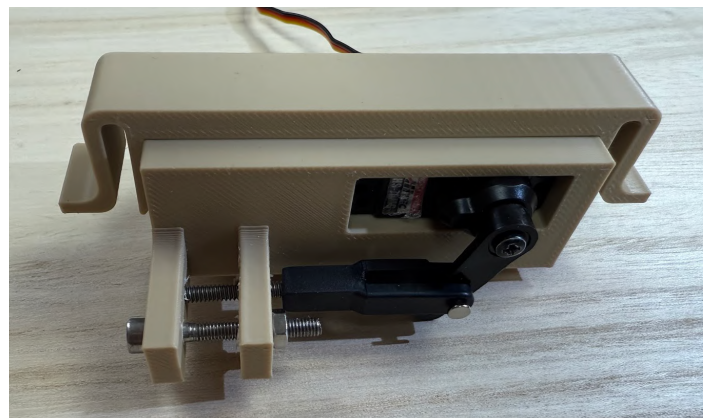


Figure 6.7: Banner deploy and release assembly.

6.3 Manufacturing Milestones

A Gantt chart with both planned and actual manufacturing milestones was created to ensure on-time task completion. As shown in the chart, subteams worked in tandem. Only the schedule for the first prototype is displayed below; similar timelines were completed for the other prototypes and the competition plane.

Table 6.1: Manufacturing Gantt chart.

| Manufacturing 25-26 Milestones | Nov | Dec | Jan | Feb | Mar | Apr | | | | | | | | | | | | | | | | | | | | |
|--------------------------------|-----|-----|-----|-----|-----|-----|----|----|----|---|----|----|----|---|---|----|----|---|---|----|----|----|---|----|--|--|
| | 2 | 9 | 16 | 23 | 30 | 7 | 14 | 21 | 28 | 4 | 11 | 18 | 25 | 1 | 8 | 15 | 22 | 1 | 8 | 15 | 22 | 29 | 5 | 12 | | |
| Prototype 1 | | | | | | | | | | | | | | | | | | | | | | | | | | |
| CAD | | | | | | | | | | | | | | | | | | | | | | | | | | |
| Wing/Tail | | | | | | | | | | | | | | | | | | | | | | | | | | |
| Hotwire Wing | | | | | | | | | | | | | | | | | | | | | | | | | | |
| Hotwire Tail | | | | | | | | | | | | | | | | | | | | | | | | | | |
| Composite Layup | | | | | | | | | | | | | | | | | | | | | | | | | | |
| Fuselage | | | | | | | | | | | | | | | | | | | | | | | | | | |
| CNC Mill Mold | | | | | | | | | | | | | | | | | | | | | | | | | | |
| Composite Layup | | | | | | | | | | | | | | | | | | | | | | | | | | |
| Laser-cut Bulkheads | | | | | | | | | | | | | | | | | | | | | | | | | | |
| Assembly | | | | | | | | | | | | | | | | | | | | | | | | | | |
| Payload | | | | | | | | | | | | | | | | | | | | | | | | | | |
| Laser-cut Duck "burgers" | | | | | | | | | | | | | | | | | | | | | | | | | | |
| Assemble Burgers | | | | | | | | | | | | | | | | | | | | | | | | | | |
| 3D Print Banner Mechanisms | | | | | | | | | | | | | | | | | | | | | | | | | | |
| Cut Banner | | | | | | | | | | | | | | | | | | | | | | | | | | |
| Final Assembly | | | | | | | | | | | | | | | | | | | | | | | | | | |
| Add Controls | | | | | | | | | | | | | | | | | | | | | | | | | | |
| Add Propulsion and Avionics | | | | | | | | | | | | | | | | | | | | | | | | | | |
| Systems Check | | | | | | | | | | | | | | | | | | | | | | | | | | |
| Test Flight | | | | | | | | | | | | | | | | | | | | | | | | | | |

7. Testing Plan

This chapter outlines the testing plan for the Johns Hopkins Design, Build, Fly team for the 2025-2026 AIAA Design Build Fly competition. The plan handles both ground and flight tests, designed to verify the aircraft's performance, identify areas for improvement, and ensure mission success. The testing process is iterative, with data from each test informing refinements to subsequent prototypes until the final competition aircraft is finalized.

7.1 Component and Ground Test Plan

Before the first prototype takes flight, rigorous ground testing is conducted on individual components and subsystems to verify their functionality and structural integrity. This phase aims to reduce risks in the flight-testing process and to identify potential issues early. The ground test plan includes both qualitative assessments and quantitative measurements.

7.1.1 Wing Structural Test

Objective: To verify the structural integrity of the wing spar and its ability to withstand expected flight loads with a safety factor.

Schedule: Completed before the first prototype assembly

Procedure: Weights, equivalent to twice the expected maximum flight load (accounting for a safety factor of 2), will be suspended at multiple locations along the wing spar. Deflection and any signs of structural failure will be observed and recorded.

Data Collected: Deflection measurements at various points along the spar under load.

Application: The data will be compared to theoretical calculations to validate the structural model and ensure the spar can handle the anticipated loads during flight. If the deflection exceeds the allowable limit, the spar design will be reevaluated.

7.1.2 Wing-Fuselage Joint Test

Objective: To verify the strength and integrity of the joint between the wing and the fuselage.

Schedule: Completed before the first prototype assembly.

Procedure: A load will be applied to the wing to simulate flight loads while the joint between the wing and the fuselage is inspected for any signs of stress, cracking, or separation. The load will be increased incrementally to determine the joint's ultimate strength.

Data Collected: Load applied and observations of the joint's condition at each load increment.

Application: This test ensures the wing-fuselage joint can withstand the stresses of flight. If the joint shows weakness, the design will be modified and retested.

7.1.3 Propulsion System Test:

Objective: To characterize the performance of the chosen motor, ESC, and propeller combination and validate the static thrust predictions.

Schedule: Completed before the first prototype assembly.

Procedure: The motor and propeller will be mounted on a static thrust stand. Thrust measurements will be taken at various throttle settings with different LiPo batteries (6-cell and 8-cell) and propellers. Simultaneously, current draw and voltage will be measured to calculate power consumption.

Data Collected: Static thrust, current draw, voltage, and power consumption at various throttle settings.

Application: The data will be used to verify static thrust predictions and determine the optimal propeller and battery combination to maximize thrust and efficiency. This information will be crucial for calculating climb rates and estimating flight endurance. Wind tunnel testing will follow to gather in-flight thrust data.

7.1.4 Control Surface Test:

Objective: To verify the range of motion and effectiveness of the control surfaces (ailerons, elevator, rudder).

Schedule: Completed before the first prototype assembly.

Procedure: The control surfaces will be actuated through their full range of motion. The angles of deflection will be measured, and the forces required to move them will be recorded.

Data Collected: Control surface deflection angles and actuation forces.

Application: The data will be used to ensure that the control surfaces have a sufficient range of motion for effective control and that the actuation forces are within reasonable limits.

7.1.5 Radio Control System Test:

Objective: To verify the range and reliability of the radio control system.

Schedule: Completed before the first prototype assembly.

Procedure: The radio control system will be tested at increasing distances to determine the maximum range at which reliable control can be maintained.

Data Collected: Maximum control range.

Application: The data will be used to ensure that the radio control system has sufficient range for safe operation during flight tests and competition.

7.1.6 Banner Release and Deploy Mechanism Test:

Objective: To verify the reliable and consistent operation of the banner release and deploy mechanism.

Schedule: Conducted after the first prototype assembly and ground testing, and concurrently with ground mission testing. Further testing will occur during M3 flight tests.

Procedure: The banner will be attached to the aircraft, and the deploy mechanism will be activated repeatedly. The deployment will be observed and recorded, noting any issues with the mechanism's function, such as jamming, delayed deployment, or unintended deployment. The team will also ensure the banner's logo remains visible while deployed. The force required to deploy the banner will also be measured. The same process will be repeated to test banner release.

Data Collected: Success/failure of each deploy/release attempt, time taken for deploy/release, force required for deploy/release, and video recordings of the deploy/release.

Application: This test is crucial for ensuring the banner can be reliably deployed during Mission 3. Any problems identified will lead to redesign and retesting of the deployment and release mechanism. The data will be used to optimize the release timing and ensure a clean separation between the aircraft and the banner. The force measurement ensures the servos have adequate power.

7.1.7 Ground Mission Test:

Objective: To practice and optimize the ground mission procedures, including payload attachment, fuel tank installation, and battery insertion, within the 5-minute time limit.

Schedule: Conducted after the first prototype assembly (Week 10).

Procedure: The team will practice the ground mission procedures repeatedly, timing each step and identifying any bottlenecks.

Data Collected: Time taken for each step of the ground mission.

Application: The data will be used to refine ground mission procedures and ensure the team completes the mission within the allotted time.

7.2 Flight Test Plan

Following successful ground testing, the aircraft will undergo a series of flight tests to evaluate its performance in real-world-use conditions. These tests will be conducted in a controlled environment and will progressively increase in complexity.

7.2.1 Initial Flight Tests (Unloaded):

Objective: To verify the aircraft's basic flight characteristics, including takeoff, level flight, turns, and landings, without any payload.

Schedule: Conducted after the first prototype assembly and ground testing (Week 10 of the schedule).

Procedure: The aircraft will be flown in a controlled environment, and its performance will be evaluated by the team's pilots.

Data Collected: Qualitative observations of flight characteristics, including stability, control response, and landing behavior.

Application: The data will be used to identify any initial issues with the aircraft's design or control systems.

7.2.2 Mission 2 Flight Tests (Charter Flight):

Objective: To evaluate the aircraft's performance with the Mission 2 payload (4.8 lb of rubber ducks and hockey pucks).

Schedule: Conducted after successful initial flight tests (Week 12 of the schedule).

Procedure: The aircraft will be flown with the Mission 2 payload, and its performance will be evaluated for speed, stability, and fuel consumption.

Data Collected: Flight speed, fuel consumption, and lap times.

Application: The data will be used to optimize the aircraft's performance for Mission 2 and ensure it achieves the target lap times and fuel efficiency.

7.2.3 Mission 3 Flight Tests (Banner Flight):

Objective: To evaluate the aircraft's performance in Mission 3, including the deployment and release of the banner.

Schedule: Conducted after successful Mission 2 flight tests (Week 14 of the schedule).

Procedure: The aircraft will be flown with the banner, and the deployment and release mechanism will be tested. The banner's ability to fly with the logo visible will also be tested.

Data Collected: Lap times, banner deploy accuracy, banner release accuracy.

Application: The data will be used to optimize the aircraft's performance for Mission 3 and ensure the successful deployment and release of the banner.

7.2.4 Data Logging and Analysis:

Throughout the flight testing process, a microcontroller equipped with an array of sensors (accelerometers, gyroscopes, an altimeter, a GPS receiver, and an airspeed sensor) will be installed on the aircraft to capture data logs. This data will be analyzed to assess the accuracy of the models used to optimize the design variables.

7.3 Test and Flight Checklists:

The following checklists will be used for ground and flight testing to ensure consistency and thoroughness:

JHU DBF Pre-Flight Checklist

Pilot: _____

Date: _____

Location: _____

Airframe: _____

Configuration: _____

Battery: _____ Cell count: _____ Capacity: _____

Motor and Prop Used: _____

Takeoff Weight (measured or best estimate): _____

Windspeed: _____ Takeoff direction: _____ Temperature: _____

Other Conditions: _____

Fuse uninstalled:

- o Control linkages present and secured
- o No physical damage to aircraft
- o Receiver antennae at right angles
- o Propulsion and receiver batteries charged
- o Transmitter(s) charged and operational with receiver(s)
- o CG in proper location. Location: _____
- o Control surfaces move freely and trimmed correctly
- o Fail-safes working properly
- o Install fuse and confirm propulsion is working properly with no propeller wobble while restraining the aircraft with the tail hook

Mission 2 - Mission 3:

- o Pax and cargo are attached and secured
-

Takeoff Notes: _____

Flight Duration: _____

Flight Notes: _____

Other Notes: _____

8. Performance Results

8.1 Wing

To test the bending of the wing, each wingtip was supported while different amounts of weight were added to a toolbox attached to the center of the wing. The wing withstood 40 lb of weight with no visual deflection in the center, indicating the wing structure would be ready for in-flight load. Figure 8.1 shows the wing structure undergoing the deflection test.



Figure 8.1: Wing deflection test.

8.2 Empennage

The vertical stabilizer was also tested under increasing loads applied to one end, with the other end clamped to the table. It withstood the force from a 3-liter bottle (approximately 7.5 lb) without significant end deflection (Figure 8.2). The vertical stabilizer was then deemed structurally capable of withstanding the loads encountered in flight. Similar tests were performed on other tail components, including the horizontal stabilizer, rudder, and elevator, all of which withstood a reasonable amount of force without noticeable deformation.

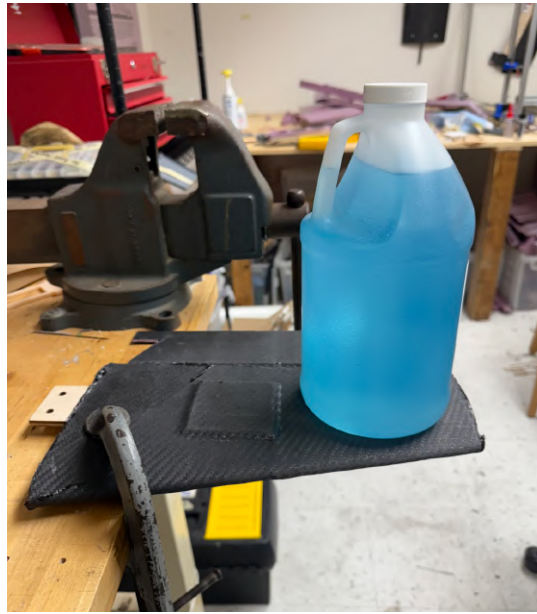


Figure 8.2: Vertical stabilizer bending test.

8.3 Fuselage

To ensure that the fuselage could withstand the thrust exerted by the motor, a spring scale was attached to the motor shaft, with a tension force of 30 lb, equal to the maximum thrust exerted by the motor multiplied by a 1.5 safety factor. There was no noticeable deformation, and so the fuselage and motor attachment were deemed adequate for flight. Figure 8.3 shows the thrust deformation test where one person was holding the rear section of the fuselage to counteract the spring force.



Figure 8.3: Fuselage thrust deformation test.

8.4 Landing Gear

To ensure the landing gear could withstand the forces it would experience, drop tests were conducted (Figure 8.4). The bottom of the landing gear wheels were lifted 12" off the ground without payload and then dropped.

Other drop tests were conducted from 3" to 5" with the full payload weight, making the weight of the aircraft 15.2 lb. Because it endured these conditions, it was determined that the landing gear's strength was sufficient for all missions.



Figure 8.4: Landing gear drop test.

9. Bibliography

- [1] 2025-26 *design, build, fly rules*. Available at:
<https://aiaa.org/wp-content/uploads/2025/08/2026-DBF-Rules.pdf> (Accessed: 18 February 2026).
- [2] Python: A dynamic open source programming, Python Software Foundation [online],
<https://www.python.org>.
- [3] D. Raymer, in Aircraft Design: A Conceptual Approach, Reston, Virginia, AIAA, 1999
- [4] "Rubin, D., & Morr, G. (1978). *Drag Investigations of Towed Target Banners* (Technical Report ADA065479). U.S. Army Missile Research and Development Command, Redstone Arsenal, AL."
- [5] AVL, <https://web.mit.edu/drela/Public/web/avl/>.
- [6] Ansys Composite PrepPost (ACP) for developers (no date) *Ansys Developer Portal*. Available at:
<https://developer.ansys.com/docs/acp> (Accessed: 20 February 2026).
- [7] Engineered carbon fiber composite sheets, tubes and structural components: Made in USA (no date) *DragonPlate*. Available at:
https://dragonplate.com/?gad_source=1&gad_campaignid=19594441824&gbraid=0AAAAAD_gw0tQI5YFZ2fpl_-VdKzKYCjjM&gclid=Cj0KCQiAqeDMBhDcARIsAJEbU9RzOvF48xEJoU97ELUmvgvIJ5gwrONQdTpngPWIRy0k7INLQYmqrjhEaAjYaEALw_wcB (Accessed: 20 February 2026).
- [8] Ansys CFX | Industry-leading CFD Software. Available at:
<https://www.ansys.com/products/fluids/ansys-cfx> (Accessed: 20 February 2026).
- [9] Performance data (2025) APC Propellers. Available at:
<https://www.apcprop.com/technical-information/performance-data/?v=7516fd43adaa> (Accessed: 18 February 2026).